REPUBLIC OF TURKEY
ISTANBUL GELISIM UNIVERSITY
INSTITUTE OF GRADUATE STUDIES

Department of Electrical and Electronics Engineering

SIXTH-GENERATION NETWORKS BACKHAUL THROUGH OPTICAL FREE SPACE

Master Thesis

MOHAMMED KADHIM ALFALIH

Supervisor

Assoc. Prof. Dr. Indrit MYDERRIZI

Istanbul – 2022

THESIS INTRODUCTION FORM

Name and Surname	**:**	Mohammed Kadhim ALFALIH
Language of the Thesis	**:**	English
Name of the Thesis	**:**	Sixth-Generation Networks Backhaul Through Optical Free Space
Institute	**:**	Istanbul Gelisim University Institute of Graduate Studies
Department	**:**	Electrical and Electronics Engineering
Thesis Type	**:**	Master
Date of the Thesis	**:**	21/11/2022
Page Number	**:**	91
Thesis Supervisors	**:**	Assoc.Prof. Dr. Indrit MYDERRIZ
Index Terms	**:**	(FSO)Free Space Communication, 6G Sixth Generation Communication, (OWC) Optical Wireless Communication
Turkish Anstract	**:**	Araştırmada, altıncı nesil ağlar ve FSO teknolojilerinin ana taşıyıcı mobil ağlarda kullanım olasılığı, avantajları, türleri ve dezavantajları açısından tartışılmış ve incelenmiştir.
Distribution List	**:**	1. To the Institute of Graduate Studies of Istanbul Gelisim University 2. To the National Thesis Center of YÖK (Higher Education Council)

Signature

Mohammed Kadhim ALFALIH

REPUBLIC OF TURKEY
ISTANBUL GELISIM UNIVERSITY
INSTITUTE OF GRADUATE STUDIES

Department of Electrical and Electronics Engineering

SIXTH-GENERATION NETWORKS BACKHAUL THROUGH OPTICAL FREE SPACE

Master Thesis

MOHAMMED KADHIM ALFALIH

Supervisor

Assoc. Prof. Dr. Indrit MYDERRIZI

Istanbul – 2022

Dedicated to

My first and inspiring teacher. You are still with me in every step of my success. Even if you are gone from this life... My father

To the symbol of sacrifice that still stands by my side... My mother

To everyone who was with me. And they were the reason for my progress.

I dedicate my research to you

DECLARATION

I hereby declare that in the preparation of this thesis, scientific ethical rules have been followed, the works of other persons have been referenced in accordance with the scientific norms if used, there is no falsification in the used data, any part of the thesis has not been submitted to this university or any other university as another thesis.

Mohammed Kadhim ALFALIH

…/…/2022

TO ISTANBUL GELISIM UNIVERSITY

THE DIRECTORATE OF GRADUATE EDUCATION INSTITUTE

The thesis study of Mohammed Kadhim Falih ALFALIH titled as Sixth-Generation Networks Backhaul Through Optical Free Space has been accepted as MASTER in the department of Electrical- Electronics Engineering by out jury.

Director _____

Assoc. Prof. Dr. Indrit MYDERRIZI

(Supervisor)

Member _____

Asst. Prof. Dr. Serkan GONEN

Member _____

Asst. Prof. Dr. A.F.M. Shahen SHAH

APPROVAL

I approve that the signatures above signatures belong to the aforementioned faculty members.

... / ... / 20..

Prof. Dr. Izzet GUMUS

Director of the Institute

SUMMARY

In the following research, the sixth-generation networks and the possibility of using FSO technologies in backhaul mobile networks in terms of advantages, types, and disadvantages were discussed and studied.

wireless optical communications are introduced as a suggested replacement for optical connections and radio frequencies. OWC system analysis models are proposed in association with climatically variable settings.

The recommended site connects the continents of Asia and Europe via Istanbul, where the system was evaluated using the Gamma-Gamma model as a probablity model for predicting different forms of weather turbulence. The results of the analysis of weather data for the region and geographic location indicate that the connection can be made for most of the year.

An overview was provided to exhibit the most important aspects of the research conducted for this thesis. We were able to provide context for our investigation by focusing on the need for 6G standards types, characteristics, and historical overview of OWC and its comparison with radio frequencies, and an in-depth look at how FSO technology may be used to meet these needs. following that, we analyzed the primary restrictions confronting FSO researchers who are striving to assess the feasibility, reliability, and efficiency of adopting optical wireless communication. Finally, we spoke about the most recent developments in this technology and the firms that are now engaged in developing it.

Next, the most important theories utilized in the study of FSO systems, including the Gamma-Gamma Model, Negative Exponential Model, K-distribution, and Lognormal Model, were discussed (refractive index structure, Scintillation Index) finally an equation was developed. for estimating communication quality, which is based on the attenuations estimated in response to local weather conditions including fog, snow, rain, and smoke. This equation is used to determine the quality of the FSO link's communication by investigating and figuring out what kind of network may be set up in response to a certain weather trend. Then, the characteristics of the system (C_n^2 & SI) were reviewed, where the weather turbulence was from weak to strong, as well as variations

from weak to saturated according to weather conditions throughout the year in the link region. The variables' values were strongly influenced by the ambient temperature, where the turbulence was weak to moderate at the lowest temperatures, in contrast to the values recorded at the highest temperatures, in which the turbulence was strong with fluctuations from strong to saturate. All three of these weather phenomena (rain, snow, and fog) were taken into account in the gamma-gamma model selection process. There were also system losses due to attenuations (molecular and geometric), where geometric attenuation was most detrimental to the transmission of information. For the abovementioned reasons, the value was lowered by less than 10 dB by affecting variables; the width of the beam is 1 mrad and the capture area is 0.2 m. The link margin remained steady throughout the year, notably during the time of snow cessation from April to November.

Keywords : (FSO)Free Space Communication, 6G Sixth Generation Communication, (OWC) Optical Wireless Communication.

ÖZET

Aşağıdaki araştırmada, altıncı nesil ağlar ve FSO teknolojilerinin ana taşıyıcı mobil ağlarda kullanım olasılığı, avantajları, türleri ve dezavantajları açısından tartışılmış ve incelenmiştir.

Optik bağlantılar, radyo frekansları, sistem analiz modelleri için önerilen bir yedek olarak ve iklimsel olarak değişken bir ortamda önerilen bir ilişki olarak.

Önerilen site, Asya ve Avrupa kıtalarını İstanbul üzerinden bağlamaktadır; burada sistem, farklı hava türbülansı biçimleriyle başa çıkmak için uygun bir model olarak Gamma-Gama modeli kullanılarak değerlendirilmiştir, bölge ve coğrafi hava durumu verilerinin analiz sonuçları konum, bağlantının yılın çoğu için yapılabileceğini gösterir.

Bu tez için yürütülen araştırmanın en önemli yönlerini sergilemek için bir genel bakış sunulmuştur. 6G standartlarına duyulan ihtiyaca odaklanarak araştırmamız için bağlam sağlayabildik. OWC'nin türleri, özellikleri ve tarihsel görünümü ve radyo frekanslarıyla karşılaştırılması. FSO teknolojisinin bu ihtiyaçları karşılamak için nasıl kullanılabileceğine derinlemesine bir bakış Bunu takiben, optik kablosuz iletişimi benimsemenin fizibilitesini, güvenilirliğini ve verimliliğini değerlendirmeye çalışan FSO araştırmacılarının karşılaştığı birincil kısıtlamaları analiz ettik. Son olarak, bu teknolojideki en son gelişmelerden ve şu anda onu geliştirmekle meşgul olan firmalardan bahsettik.

Bunu takiben, Gama-Gama Modeli, Negatif Üstel Model, K-dağılımı ve Lognormal Model dahil olmak üzere FSO sistemlerinin çalışmasında kullanılan en önemli teoriler tartışıldı (kırılma indeks yapısı, Parıldama İndeksi) Son adım: tahmin denklemi sis, kar, yağmur ve duman gibi yerel hava koşullarına yanıt olarak tahmin edilen zayıflamalara dayanan iletişim kalitesi. Bu denklem, FSO bağlantısının iletişiminin kalitesini belirlemek için kullanılır. belirli bir hava durumu eğilimine yanıt olarak ne tür bir ağ kurulabileceğini araştırmak ve bulmak. Ardından, bağlantı bölgesinde hava türbülansının zayıftan güçlüye doğru olduğu ve yıl boyunca hava koşullarına göre zayıftan doyguna doğru değişimlerin olduğu sistemin özellikleri (C_n^2 & SI) incelenmiştir. Değişkenlerin değerleri, ortam sıcaklığından güçlü bir şekilde etkilenmiştir. Türbülansın güçlüden doyguna doğru dalgalanmalarla güçlü olduğu en yüksek sıcaklıklarda kaydedilen değerlerin aksine, en düşük sıcaklıklarda türbülansın zayıftan orta dereceye kadar olduğu yerler. Bu hava olaylarının üçü de (yağmur, kar

ve sis) gama-gama modeli seçim sürecinde dikkate alındı. Geometrik zayıflamanın bilgi iletimi için en zararlı olduğu durumlarda (moleküler zayıflama, geometrik) kaynaklanan sistem kayıpları da vardı. Değişkenler etkilenerek değer 10 dB'den daha az düşürülmüştür, kirişin genişliği 1 mrad ve yakalama alanı 0.2 m'dir. Bağlantı marjı, özellikle Nisan'dan Kasım'a kadar olan karların kesildiği dönemde, yıl boyunca sabit kaldı.

Anahtar Kelimeler : FSO)Boş alan iletişimi , 6G Altıncı Nesil İletişim, (OWC)optik kablosuz iletişim.

TABLE OF CONTENTS

CHAPTER THREE

THE CHARACTERIZATION OF AN OPTICAL CHANNEL IN AN ADVERSITY ENVIRONMENT

ABBREVIATIONS

FSO	Free space optical
BER	Bit error rate
6G	The sixth generation of communications
RF	Radio frequencies
OWC	Optical wireless communications
AI	Artificial Intelligence
VLC	Visual Light Communications
IR	Infrared
OCC	Optical camera communications
LiFi	Wireless networking with light
MIMO	Multi-Input Multi-Output
SIMO	Single-Input Multi-Output
IOT	Internet of things
LOS	Line-Of-Sight
PDF	Probability density function
OOK	On Off Keying Modulation
IM/DD	Intensity-Modulation/Direct-Detection
M_{link}	Link margin
AGC	Automatic gain control
AM	Amplitude modulation

Q-Ary	Multi-mode
PPM	Pulse-position modulation
BPSK	Binary phase shift keying
BPSK SIM	Binary Phase Shift Keying Simulation
APD	Avalanche Photodiode
TDM	Time divided modulation
MRC	Maximal ratio combining
EGC	Equal gain combining
PD	Photodiode
PE	Pointing error

LIST OF SYMBOLS

I_0	Mean Received Irradiance
σ_x^2	Rytov parameter
L_{p}	Horizontal Distance
C_n^2	Index Of Refraction Structural
k	Wavenumber
L	Length Of The Link
I_x	Large scale turbulent eddies
I_y	Small scale turbulent eddies
SI	Scintillation index
β	Characterize The Irradiance Fluctuation
α	Characterize The Irradiance Fluctuation
M	Mean Irradiation
Γ (.)	Gamma Function
$\mathbf{K}_{\alpha}$**(.)**	Bessel Function
ω_z	Beam Waist
erf(.)	Error Function
h	channel state
r	Proportion Of The Pointing Error
σ_N	Noise Standard Deviation
RMS	Root Mean Square
$V(h)$	Wind Speed

w_g	Ground Wind Speed
w_s	Beam slew rate
P	Air pressure
T	Air temperature
C_T^2	Temperature Structure
l_0	Inner scales of the atmospheric turbulence
L_0	Outer scales of the atmospheric turbulence
r	Distance
I	Intensity of the optical
P_e	Transmitter's power
S_r	Recipient's responsiveness
Att_{geo}	Geometrical loss
Att_{mol}	Loss at the molecules
P_{tot}	System Loss
θ	Divergence
$\mathbf{R}$	Distance Between Transmitter- Receiver
s_{capture}	Receiver's Capture Area
α_{fog}	Fog Attenuation
$\mathbf{V}$	Visibility Range
λ	Wavelength
λ_o	Visibility range reference

q	scattering size distribution coefficient
A	Rain Attenuation
k	Rain parameters
a	Rain parameters
R	Rate Of Rainfall
$\alpha_{S_{\text{now}}}$	Snow attenuation
a	Snow parameters
b	Snow parameters
τ	Haze attenuation
σ	propagation distance
l	specific attenuation per length

LIST OF TABLES

LIST OF FIGURES

ACKNOWLEDGEMENTS

This thesis wouldn't be feasible without the help of many individuals, and I want to express my gratitude to them all. To begin, I'd like to thank Professor INDRIT MYDERRIZI for giving me an outstanding chance to study free-space communication. My studies and my life were considerably enriched by Dr. AHMED AMIN SOLAMIN's infinite supply of research ideas and motivation. Visiting Gelisim University was a life-changing experience.

CHAPTER ONE

INTRODUCTION

1.1 Motivation of Research

Speaking of the near future, more than two-thirds of the world's population will be connected to the Internet through mobile devices, according to a study conducted by Cisco. Subscriptions to mobile phones throughout the world will increase from 5.1 billion in 2018 to 5.7 billion in 2023, representing 71% of the global population, according to the International Telecommunication Union. It will be 13 times faster than a typical mobile connection today, and 5G is expected to be available. The typical 5G connection speed will be 575 Mbps. About 300 million people are expected to download mobile apps, and they will be downloaded 299.1 billion times worldwide, according to estimates. The most popular downloads will be social networking, gaming, and business software. Broadband service speeds are predicted to increase by more than double. According to Cisco, the average fixed broadband speed will more than triple from 45.9 Mbps, and mobile network connections will average 13.2 Mbps, rising to 43.9 Mbps by 2023 (Barnett, 2018) . The increasing number of mobile users is putting a strain on cellular networks' ability to transfer data. Backhaul optimization is becoming just as important as radio infrastructure investment. Backhaul costs and capacity issues are being alleviated by new transmission technologies, topologies, and network design (Chia, 2009). Microwave radio connections or optical fibers are the most common forms of mobile backhauling used to connect radio controllers and base stations. Better ways to deal with capacity and coverage are needed that is, to increase spectral effectiveness owing to an increase in the use of mobile customers in addition to the implementation of cellular network systems. When constructing a mobile backhaul network for 4G cellular networks, numerous issues must be taken into account. Additionally, 5G-based mobile backhaul networks must fulfill ultra-low latency criteria of 1 ms or less and have highly dense network capabilities. Fast Ethernet/Internet technologies and optical fiber lines, represent Over 90% of all backhaul networks that work at speeds between T1-1.544 Mbits/s and E1-2.048 Mbits/s (Sharma, 2021). As for the remaining 6%, they rely mostly on microwave radio or optical fiber connectivity (Tipmongkolsilp, 2010). Referring to(6G) backhauls

are predicted to have better bit rates and reliability as a result of the enormous number of people that will be using the central network. Optical and microwave backhaul have been proposed as potential options for backhaul networks of the future. To address issues and increase the cost of backhaul effectiveness, (FSO) free space optical communication is evolving as an appealing high-rate transmission, low-cost, technology for 6G cellular networks. It is not always feasible to establish an optical fiber backhaul network because of distance's cost, Tiny cell networks may also be unable to make use of fiber optic links because of the prohibitive cost of Front/Backhaul (Zong, 2019). In terms of transmission and reception, An FSO system is equivalent to an optical fiber network because the FSO system may transport data at the same rate as an optical fiber system. Optical fiber networks and FSO serve as good backhaul and fronthaul technologies for 6G. This Thesis will explore the benefits and drawbacks of employing FSO connection to attain a high degree of efficiency, as well as how it may potentially be used in the future.

1.2 The Essentials of 6G

By 2030, 6G will be widely available. Improved information transmission is expected data speeds of up to 1 Tbps in the next generation (6G), it communicates at terahertz frequencies and has a microsecond latency. One of the goals of 6G networks is to provide global reach by integrating satellite and underwater communications. The use of modern materials would significantly increase the system's energy efficiency and allow the development of long-term networks designed to be energy efficient. The following is an overview of the 6G features: (Huang T. Y., 2019).

- High-speed data transfer (up to 1Tbps)
- Minimal latency.
- Exceptional efficiency in energy use.
- Better global network access.
- Intelligent and reliable networking.

Figure 1.1, shows the next generation of information technology, including edge computing and big data, is on the rise. Because of 5G's convergence with (AI) use of industrial and transportation technologies, it has expedited these sectors' progress as

part of the 6G network, to respond to the deep convergence of the Internet of Things (IoT) and various industries. Everything is invisibly connected and closely spaced in order to maximize efficiency. The architecture of the 6G network faces many challenges, terahertz waves, peak power, and other technical problems are among the most important issues.

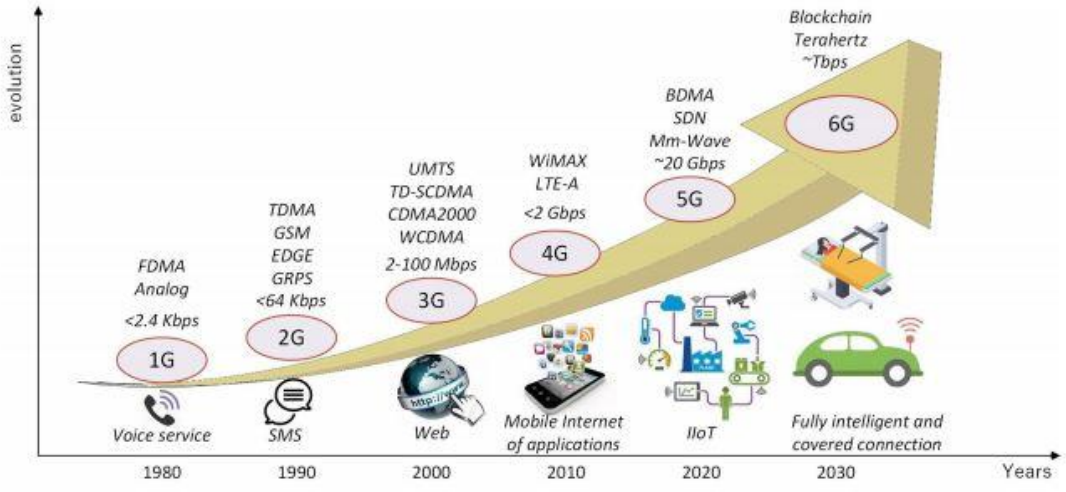

Figure 0.1: Evolution of mobile wireless systems (Huang ve diğerleri, 2019)

Before 6G communication systems can be used successfully, several technical problems need to be solved :

- Massive MIMO 6G upgrading will need a new design because of hardware limitations, communication techniques, and algorithm challenges.

- Terahertz signal sensitivity: High THz frequencies allow for a large data rate however, the large propagation loss and minimal absorption by the atmosphere make the transmission of data over long distances in the THz bands difficult.

- Effective spectrum management: the scarcity of spectrum and worries about interference for the most efficient use of resources, spectrum management is necessary.

- Connectivity for High-Capacity Backhaul: 6G will have a dense access network to High-speed backhaul communication through optical fiber or

FSO networks is conceivable. There will be many fast data networks for various user categories, which must manage massive data quantities.

The deployment of 6G networks may take several forms, one of which being wireless optical networks, which can meet all of the requirements of low-cost, time-consistent, high-bandwidth networking communication to meet the backhaul needs for 6G (Zong, 2019).

1.3 Optical Wireless Communication (OWC)

Using light to communicate goes back a long way in human history since the Romans and Greeks used mirrors in the 8th century to reflect sunlight from place to place (Bell, 1880). In 1792, Claude Chapper devised the optical telegraph, a means of transmitting information (Bouchet O. S., 2010). The blinking lights were used for ship-to-ship communication for many years. The process of evolution started by two scientists, Charles Sumner and Alexander Graham Bell, led to the invention of the photo-phone, which utilized sunlight to modulate voice via mirror vibration to transmit speech in 1880. In that experiment, sunlight was reflected off a thin mirror put at the end of a speaking tube and sent to the transmitter. The quantity of light reflected from the mirror's surface varied as words were pronounced and as the mirror shifted between convex and concave. The receiver's focal point was a parabolic mirror with selenium cells at the top. As a result, the photo-phone was the first method ever discovered for transmitting audio over the air, as shown in Fig1.2 (Goodwin, 1970).

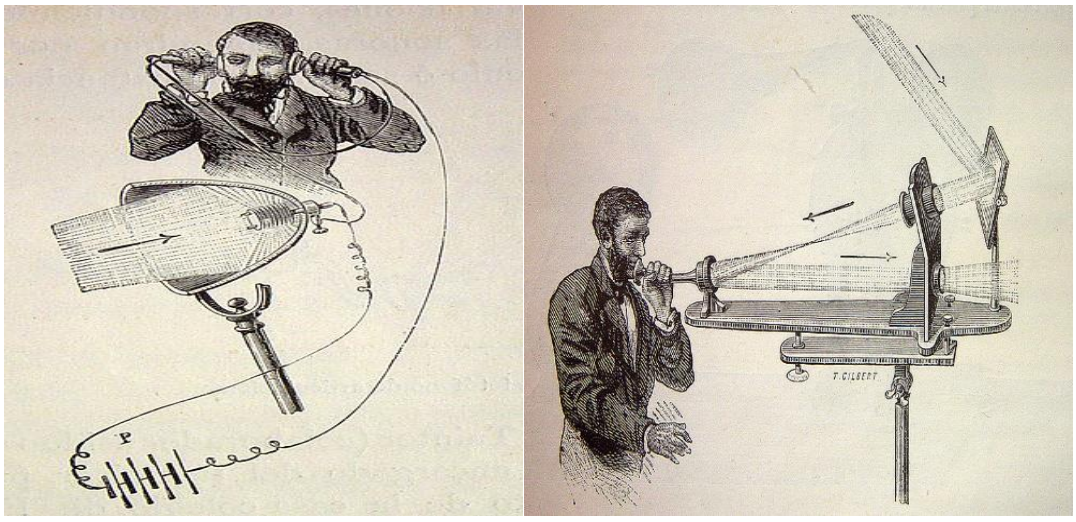

Figure 1.2. Photophone, transmitter (left), receiver (right)(Bell, y.y.)

The German Army 1935 employed tungsten filament lamps with an infrared transmission filter as the light source. In addition, high-pressure arc lights for optical communication continued to be developed by American and German military labs throughout the 1950s (Manohar, 2016). Since the advent of laser technology in 1960, high data rates were transferred across the atmosphere. In 1970, the first open space channel was launched by the Nippon Electric company with laser drivers at a wavelength of 630 nm and over long distances of around 14 km (Goodwin, 1970). A surge in academic and commercial interest in optical wireless communication (OWC) has occurred during the past several years. In light of the wide range of applications that OWC technologies may serve, they are currently available in a wide range of configurations. Below are several OWC techniques used:

1- Free space optical communications: FSO systems may be used to communicate between two fixed locations across long distances. The optical bandwidth of the FSO connection is much bigger than that of its RF counterparts, with transmission rates of up to 10 Gbps equivalents (Rodewald, 2008) .

2- Visible light communications VLC: It is possible to communicate across small distances using an optical wireless technology system by utilizing LEDs for both lighting and transmission (Bouchet O. B., 2008). In VLC, data transmission is accomplished by varying the intensity of light that is imperceptible to the naked eye.

3- Optical camera communications (OCC): Flashing light may be used as a source of information for the sensor. In the same way that high-brightness white LEDs have led to VLCs, the digital camera has led to OCCs. (Roberts, 2013)

4- Wireless networking with light (LiFi): Uses visible and infrared light to convey data at high rates (Haas, 2011) . Since its inception, the term "LiFi" has been used to refer to a new class of wireless communication that combines the advantages of visible light communication (VLC) with many additional features (Rodewald, 2008).

All the above-mentioned techniques can be utilized in integrated circuits such as optical interconnects the connection between buildings and satellite

communications. From optical interconnects inside integrated circuits to outdoor inter-building connectivity, to satellite communications, OWC may be used in a wide variety of applications depending on the range of transmission, as follows:

1- Ultra-short range: Multi-chip packages with chips packed tightly together, chip to chip (Rodewald, 2008) (Taubenblatt, 2011) .

2- OWC Short range: Underwater communications, wireless personal area network (WPAN), wireless body area network(WBAN) (Hranilovic, 2004).

3- OWC Medium range: VLC using wireless local area networks (WLANs), indoor IR, vehicle-to-infrastructure links, and inter-vehicular (Gfeller, 1979).

4- Long-range OWC: Connectors between different buildings.

5- Ultra-long range OWC: Communications between satellites and in deep space (Chan, 2003) (Hemmati, 2006).

The coverage area for personal communications can be as small as a few centimeters, but commercial applications may need a coverage area of nearly a kilometer, as shown in figure 1.3. (Borah, 2012).

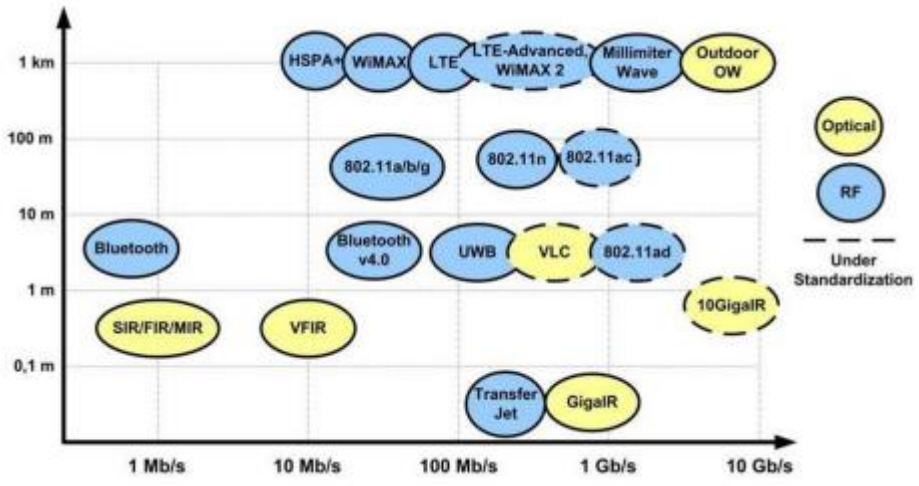

Figure 0.3. Commercial product's use of standards-defined RF and OW technologies (Borah, 2012)

Security and interference are demonstrated in Table 1.1 as a result of comparing data transmission speeds between radio frequencies and optical wireless communications.

Table 0.1. RF and OWC systems comparison

Property System	**RF**	**OWC**
Data rate	1.25 Gb/s	10 Gb/s
Bandwidth	Licensed	Not regulated
Security	Low	High
Cost	High	Low
Directionality of the beam	Low	Required
Bandwidth	Low	High
Transmitter Power	Interference	Interference & Eye safety
Noise	Systems & Other Users	Weather
Power consumption	Medium	Low
Multipath Fading	Yes	No

1.4 Free Space Optical (FSO)

When it comes to wireless communications, FSO is the most similar to optical fiber in that it allows static point-to-point communications across quite long distances (Pang, 1999). Due to its high rates of transmission through unlimed and unlicensed bandwidths, FSO communication has over the years attracted significant research attention. (LOS) the equipment uses optical bands for establishing contact links over long distances at up to 10 gigabits per second of data rate (ultraviolet, visible light, and infrared) (Schütz, 1990) . Instead of optical fiber cables, the laser beam travels through the air or space using FSO transmission. Communication between two fixed places across distances of many kilometers may be accomplished using FSO systems. When compared to RF, the optical bandwidth of the FSO connection allows for significantly larger data rates. When compared to RF, an FSO connection's optical bandwidth allows for much higher data rates and can be used with OWC devices that can send up to 10 Gbps. Experimental OWC systems can also compete with fiber optics in terms of how quickly they can transfer data (Jeong, 2002). The laser beams used in FSO devices are very narrow; there is also reusability, safety, and resistance to

electromagnetic interference. Furthermore, the FSO technology operates at a frequency exceeding 300 GHz, which is unregulated in every country, as a result, no licensing costs are required for FSO systems (Farooq, Sahu ve Gupta, 2018). Many researchers began to improve the transmission capacity and range of FSO systems for a broad variety of purposes. The technology was used in a wide range of applications, including military, civic, and deep space missions. For the time being, the visible light spectrums and IR have been used in high-speed data transfer as a remedy to RF (M Uysal ve Nouri, 2014). It will also take the lead in outdoor and indoor communications of next-generation- networks (NGN) because of the fast advancements in FSO technology (Wu, 2011) . Over the years, the interest in OWC has been mostly restricted to clandestine military applications (Begley, 1992). Many applications are possible, from ultra-short to ultra-long-range, by using FSO (M Uysal ve Nouri, 2014). There are several examples, including chip-to-chip communication, wireless area networks, metropolitan networks, wireless personal area networks, aircraft-to-aircraft, last-mile solutions backup links, deep space missions, inter-satellite linkages, and military objectives(Z Ghassemlooy, Popoola ve Rajbhandari, y.y.). There are several commercially accessible, off-the-shelf FSO products on the market with speeds ranging from a few hundred Mbps to 10 Gbps (Gohil, 2019), (Pan, Ekici ve Feng, y.y.). Prototype systems with throughputs of 100 Tbps are being demonstrated at cutting-edge research facilities (Huang H. X., 2014). There must be 10 Gbps data rates available in next-generation wireless networks. Where the number of FSO transceivers sharing hundreds of wavelengths is increasing rapidly (Pan ve diğerleri, y.y.). FSO backhaul wireless network rates of 10 Gbps have been reported in the literature. (M Uysal ve Nouri, 2014). However, laboratory tests have shown significantly greater rates in the tens of terabits per second range (Huang T. Y., 2019). FSO technology has risen in popularity due to the shrinking size of cells to a few hundred meters or less, which makes it an attractive backhaul option for connecting cells with massive wireless network capacity in the next generation. Besides that, it has a greater carrying capacity, less expensive than fiber optics. Moreover, the backhaul network's selection and development are critical, as it accounts for 30% to 50% of 4G systems' total operating expenditures (Kaushal H. K., 2011). Since it is more than half of the world's population will be electronically interconnected by 2020 (Sannibale, 2009); Therefore, there is a need for technologies with high transmission rates such as FSO technologies.

1.4.1 LIMITATIONS ON FSO

Because the benefits of FSO are straightforward to utilize, it may be used for a wide range of applications of wireless communication. Nevertheless, since FSO signals are transported via the air, they face a variety of environmental challenges, as seen in Fig. 1.4. The troposphere is the area of the atmosphere where the majority of atmospheric events occur (Fadhil, 2013). Figure .14 depicts the consequences of the limits imposed by the atmosphere, some of these restrictions are briefly addressed in the section that follows:

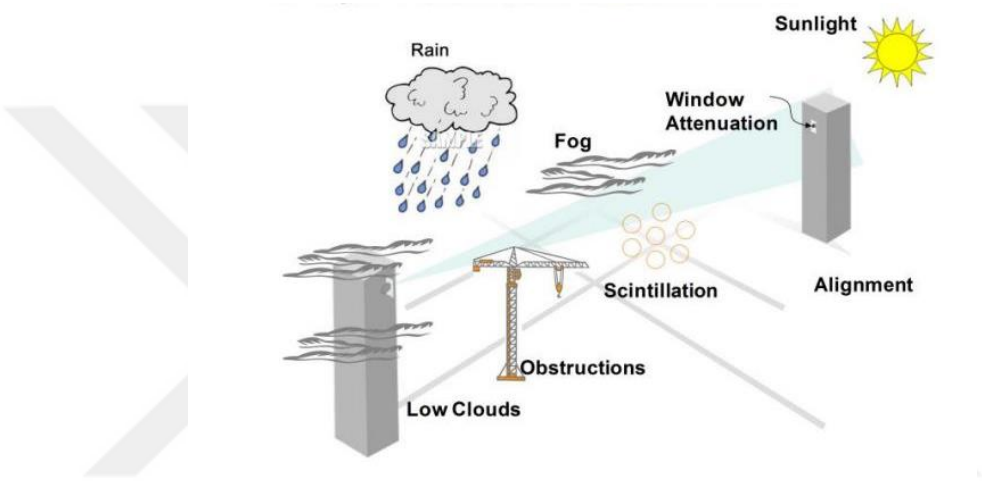

Figure 0.4. Impact of varied weather conditions on the FSO link(Pan ve diğerleri)

- Physical impediment: FSO beams cannot be sent to the receiver if there are any temporal impediments, such as the movement of birds or aircraft. It is also the construction of high-rise structures and the planting of trees that are both seen as important disruption elements in the spread of FSO. Because of this, the position of FSO transceivers must be carefully considered (Gfeller, 1979).

- Turbulence in the atmosphere: Invisible disturbances in the air arise as a result of environmental and weather-related factors, resulting in atmospheric turbulence. Wind-induced temperature and pressure changes cause air cells to oscillate and, as a result, random eddies of varying sizes form. An optical beam's behavior may be described in terms of the eddies' scale sizes after its

passage through an air current channel (Hemmati, 2006). There may be a turbulence-induced wander beam if the eddies are greater than the optical beam, and this might be a dominating effect. Random beam movement and connection failure are also likely outcomes (Kaushal H. K., 2011). Eddy sizes lower than optical beam diameters may cause fluctuations in beam irradiance. Turbulence-induced beam scintillation is the name given to this phenomenon in which the received signal is subject to temporal and spatial fluctuation due to the beam scintillation. Typically, this occurs when two or more eddies begin to interact with the transmission signal (Sannibale, 2009).

- Misalignment pointing error: Link failure is possible when there is a problem with FSO communication. Satellite tremor or platform jitter are two examples of possible causes, as well as any type of strain on electrical or mechanical components (Sannibale, 2009). Atmospheric turbulence-induced beam wander may shift the beam off its transmit path and create pointing inaccuracy (Guo, 2010). Pointing errors may lead to connection failure or a considerable reduction in received power, giving rise to significant errors in both circumstances. The assembly must be vibration-free and have enough adjustment and sufficient dynamic range and bandwidth to make up for any remaining jitter to achieve aiming precision (Tyler, 1994).

- Background noise: noises in the background are (Tyler, 1994):

    a. The atmosphere dispersed long-term background noise.
    b. Sun's and other celestial bodies' noise in the backdrop.
    c. Receiver-collected scatt light.

    Limiting the receiver's optical bandwidth reduces background noise. A single optical filter having a very narrow bandwidth of roughly 0.05 nm may be used to reduce background noise. FSO system's noise is further contributed by the dark current in the detector; shot noise in the signals and thermal noise. The overall contribution of noise includes both background and other sources (Kaushal H. &., 2015).

- Scattering loss and absorption: According to Beer's law, air absorption and scattering account for the majority of the loss (Weichel, 1990). Water, ozone molecules, and carbon dioxide are the most common air absorbers in the

visual and infrared ranges (Long, 1963). The wavelength-specific absorption occurs in the atmosphere, so the FSO communication system uses a wavelength range that has low absorption. Light scattering additionally hampers the FSO system's performance. Scattering, like absorption, is significantly influenced by wavelength. While Rayleigh scattering occurs if the air particles are tiny in proportion to the wavelength of the optical radiation. For that, the FSO must communicate utilizing visible or ultraviolet wavelengths below 1 m, and this scattering is readily observable in the case of longer wavelengths, it may be overlooked (Willebrand ve Ghuman, 2002).

- Atmospheric weather conditions: Since the optical beam passes through the atmosphere the fundamental constraints of the FSO system are dependent on the meteorological conditions. Fog, rain, snow, smog, smoke, windstorm, sand-wind, and fluctuations in turbulence intensity of the atmospheric characteristics have a significant impact on optical propagation (Arockia Bazil Raj, 2016) (Majumdar, 2010). Vapor droplets and aerosol particles, each around 100 microns across, may have an important influence on the propagation properties of an optical wave, impairing it totally and degrading the waves.

FSO connections as a result of this research, it is possible to assess the reported usage of this technology and develop models, to budget for an effective connection establishment to guarantee that FSO systems work at a predefined level of dependability.

1.5 Related and Previous Works

FSO's performance has been improved and a lot of effort to address the impacts of air turbulence has mitigated its limitations. Scientists are doing research in a variety of fields. Several scholars have investigated how turbulence impacts their performance using a range of modulation methodologies. Various modulation methods, including OOK, Subcarrier BPSK, and Q-ary PPM, are compared in the turbulence regime. Except when the order of Q in Q-ary PPM was raised, BPSK outperform others, according to the findings. Space diversity reception technique (SDRT) and complex modulation schemes, according to (Wang, Zhong, Fu ve Lin, 2009), can efficiently

decrease air turbulence transmission inefficiencies. The BPSK SIM, on the other hand, performs better in all turbulence variations(Popoola ve Ghassemlooy, 2009). When employing FSO systems with APD detectors, it is vital to pick an ideal average APD gain to reduce excessive APD noise in the receiver. In these systems, differential amplitude PPM outperforms other approaches for the same peak power(Farooq ve diğerleri, 2018; Kiasaleh, 2006). Turbulence is less likely to affect gain as the number of apertures increases. Turbulence has a substantial influence on SISO-FSO line performance. The studies (Peppas, Nistazakis, Assimakopoulos ve Tombras, 2012; Tsiftsis, Sandalidis, Karagiannidis ve Uysal, 2009) indicated that employing a large number of apertures at the transmitter and receiver can increase performance and hence FSO quality. Using the OFDM-FSO connection instead of the TDM-FSO link (Kumar ve Srivastava, 2015) can result in increased gain and enhanced receiver sensitivity. The performance of an FSO system is determined by the amplifier it employs. In terms of total performance, the optical pre-amplifier outperforms the electronic amplifier. Pre-amplification employs erbium-doped fiber amplifiers to amplify signals before they reach the photodetector, whereas electronic amplification Erbium-Doped Fiber-Amplifier(EDFA) enhances signals after they have passed through the photodetector(Cao, Brandt-Pearce ve Wilson, 2006) . To describe the parameters of the optical channel as a function of atmospheric turbulence, models have been constructed. The most commonly used statistical models to explain the atmospheric turbulence channel are Log-normal, K, and G-G distributed channel models. The G-G distribution, one of three potential distributions, is used to model atmospheric turbulence irradiance change in weak and strong turbulence regimes. When substantial turbulence is a problem, the Negative Exponential distribution is utilized. When it comes to turbulence system weaknesses, however, the log-normal distribution is used (Popoola ve Ghassemlooy, 2009; Tang ve diğerleri, 2010). The gain of the FSO system improves when many apertures are used at either the transmitter or receiver. Even yet, the Pointing Error (PE) produced by building movement diminishes FSO, cancelling out the advantages of using multiple apertures. PE's impact on FSO MIMO system Gamma-Gamma fading atmospheric fluctuation is discussed in (Kihl, y.y.) .

A comparison of equal gain combining (EGC) and maximal ratio combining (MRC) was made. Where EGC has been shown to be more susceptible to large-scale PE.

However, for mild to moderate PE, EGC is superior than MRC due to its ease of usage (Bhatnagar ve Ghassemlooy, 2016).

According to a 2018 Markets & Markets research, technology adoption will increase by 391.79% by 2025. also, The FSO market is predicted to expand by 37.5%, and the VLC industry is expected to grow almost five times by 2025. As shown in Fig 1.5, there is a predicted rise of 66.5 % overall. (Kaushal H. &., 2015)

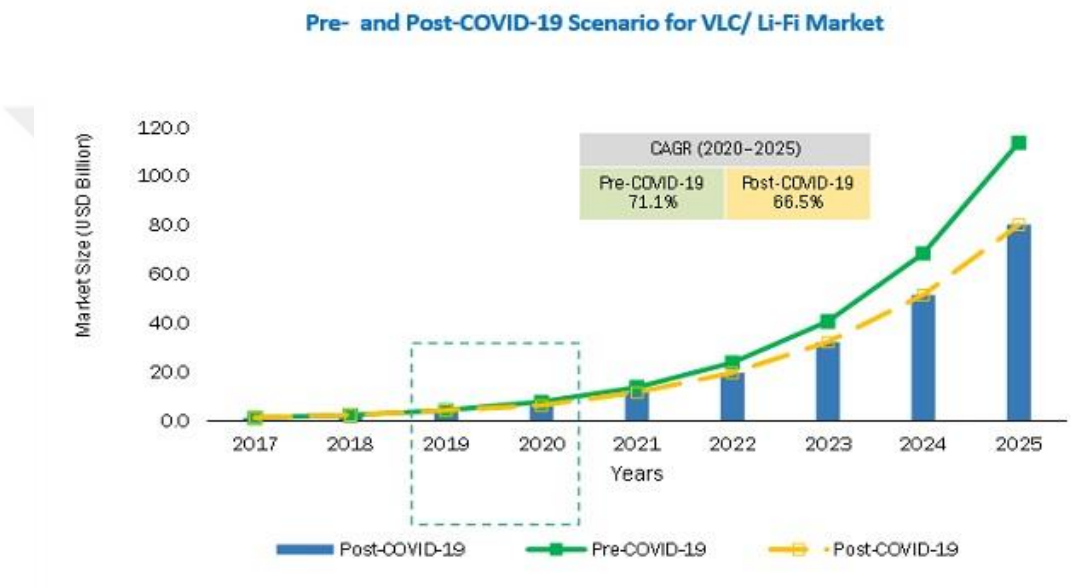

Figure 0.5.VLC market forecast for the years 2020-2025(“marketsandmarkets.com”, y.y.)

This kind of communication may be used in a wide variety of fields. As a result, light communication has enhanced its capabilities and generated significant profits in the market. Research shows that Cassidian (Germany), Canon (Japan), GeoDesy (Hungary), LightPointe Communications (USA), fSONA (Canada), and Laser ITC (Russia), among others, are now working on the production and design of FSO systems for wireless communication solutions in the outdoors. A 10 Gigabit wireless link was established at Crédit Agricole's Saint Quentin in Yvelines bank in Paris on October 16th by fSONA Networks, the firm that manufactures the fastest optical wireless solutions currently on the market, while in Vancouver, British Columbia.

Four SONAbeam 2500-Z connections were installed to replace a fiber ring connection. More than 1,600 individuals depend on this connection daily (Kumar, 2015). When it comes to 4G LTE backhaul, SONAbeam from fSONA delivered fiber-like connection at gigabit plus speeds without the time delay of running cable. Touch's Beirut location for SONAbeam. A prominent US FSO business, Northern Storm, installed an FSO connection with a 10.31 Gbps FSO link with a 1 Gbps RF backup at 238 meters. With 99.999 percent uptime in various weather conditions (Tsiftsis, 2009), the system under examination is a strong contender. Collinear's solutions for mobile, fixed, and Internet of Things (IoT) networks allow for highly flexible capabilities and effectively manage difficulties. Collinear's solutions have Up to 10 Gbps of capacity delivered by Collinear's LightCNX and AirCNX millimeter wave product lines, while the HybridCNX hybrid free-space product line can provide up to 20 Gbps of capacity (Horimai, 2005).

CHAPTER TWO

FSO SYSTEM AND CHANNEL MODELS

2.1 Introduction

In this chapter, an examination will focus on how to assess any system using the most influential theories for evaluating systems based on the climatic circumstances of the location where a communication network is formed. In addition, how can the optimal model be developed based on the primary variables, attenuation rates, and their influence on the FSO channels and methodologies used to measure the quality of communication networks.

2.2 System And Channel Models

Several channel models for free space optical communication (FSO) will be discussed, including log-normal, negative exponential, gamma-gamma, and K distributions. Where they are used to achieve the highest performance and lowest bit error rate (BER) for the unperturbed and somewhat perturbed channels. Moreover, these statistical models are used to try to describe the turbulences mathematically.

2.2.1 Negative Exponential

The number of separate scatterings gets significant within the range of high irradiance changes in the beyond and saturation regime when the connection length extends several kilometers (Bloom, 2003). The negative exponential is a model that is often utilized for simulating strong conditions turbulence. This distribution's Probability density function (PDF) is as follows:

$$p(I) = \frac{1}{I_0}\exp\left(-\frac{I}{I_0}\right) I_0 > 0 \qquad (1)$$

Where I_0 =E[I] is the mean received irradiance.

2.2.2 Log-Normal Models

The spatial coherence of coherent light radiation reduces as it passes through a turbulent medium, like the atmosphere, and cohesion degradation is governed by the

turbulence in the atmosphere. The Rytov approach was used to simulate the spatial coherence of a field in the presence of modest air turbulence; it was also used to determine the propagation distance and intensity of a turbulent channel via which coherent radiation is conveyed. Furthermore, the Rytov approximation and the log-normal turbulence model were used to simulate atmospheric turbulence. There has been a noticeable improvement in radiation fluctuation data in the low-fluctuation zone where a log-normal distribution is used to find it experimentally and to simulate atmospheric turbulence. Rytov parameter, according to the Rytov approximation, is grown indefinitely concerning the refraction index, route length in the area of weak turbulence only when $\sigma_l^2 \leq$ 0.3 (Scholz, 2016) , (Karp, 2013). As the turbulence strength rises above the weak regime, combined with longer travel distances or increasing C_n^2, the turbulent eddies produce numerous scatterings Rytov's estimation does not take into consideration (Willebrand ve Ghuman, 2002). Within the weak regime, the (SI) grows linearly with the Rytov parameter and keeps going until it reaches a value that is greater than one. It is at this point when (SI) unpredictability or heterogeneity is most prominent. When repeated scattering generates self-interference, the effect diminishes with each passing moment, and the number of Rytov parameters rises as the Rytov parameter grows closer it gets to unity. This finding goes against what the Rytov approximation predicted for the weak atmospheric domain and beyond. Where multiple scattering effects must be addressed when atmospheric turbulence intensity rises, log-normal statistics show considerable departures from experimental data in comparison to log-normal statistics.

$$p(x) = \frac{1}{\sqrt{2\pi\sigma_x^2}} \exp\left\{-\frac{(x-E[x])^2}{2\sigma_x^2}\right\} \qquad (2)$$

Where $E[x]$ is the expected value of x and σ_x^2 is the Rytov parameter, also known as the log-amplitude variance (Karp ve diğerleri, 2013).

The σ_x^2 parameter, which describes the magnitude variation in the magnitude of air turbulence, is the horizontal distance L_{p}, which is connected to the index of refraction structural parameter C_n^2 , k is the wavenumber $\frac{2\pi}{\lambda}$, L is the length of the link. The following equations describe the path taken by the equation below, can figure out how the optical radiation works.

For a plane wave, log-irradiance variance can be calculated as such:

$$\sigma_x^2 = 0.56k^{7/6}\int_0^{L_\mathrm{p}} C_n^2(x)\left(L_\mathrm{p}-x\right)^{5/6}\mathrm{d}x \quad (3)$$

As for a spherical wave, log-irradiance variance can be determined from the equation below:

$$\sigma_x^2 = 0.563k^{7/6}\int_0^{Lp} C_n^2(x)(x/L)^{5/6}\left(L_\mathrm{p}-x\right)^{5/6}\mathrm{d}x \quad (4)$$

Additionally, the expected value of irradiance can be found using equation (5):

$$E[l] = -\frac{\sigma_l^2}{2} \quad (5)$$

In figure 2.1 for various log-irradiance variance σ_l^2 values as l rises in value σ_l^2, the distribution increases in its skewness, with tails that are longer pointing toward infinity. This indicates the degree of irradiance fluctuation as channel inhomogeneity grows.

Figure 0.1. Log-normal pdf for a range of log irradiance variance

2.2.3 Gamma–Gamma Model

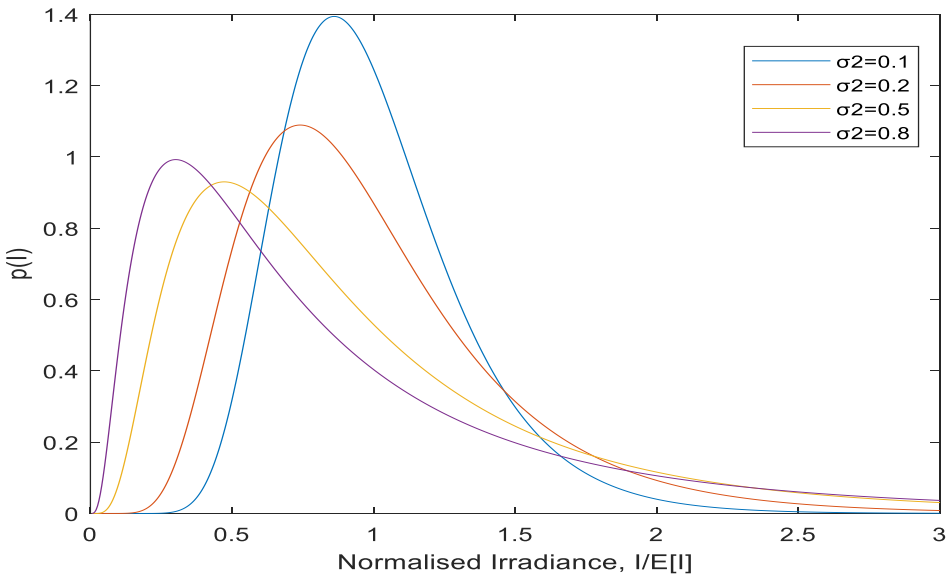

When it comes to the modification of radiation that occurs as a result of small (scattering) and large-scale impacts in a turbulent environment Gamma-Gamma model

covers all turbulence states from mild to high (Gohil, 2019). The Fresnel area is bigger than the eddies cells, the consistency radius is less, on the other hand, the turbulent edges are over the first zone of the Fresnel or the spreading disk, which is bigger than the scattering disk's or first zone. The little edges are supposed to be modulated with the bigger edges Therefore, the standardized irradiance I received is defined as two statistically independent products $I_x I_y$.(Al-Habash, Andrews ve Phillips, 2001; Andrews, 2005; Singh ve Chechi, 2019).

$$I = I_x I_y \quad (6)$$

I_x and I_y are generated by turbulent eddies on a large and small scale. respectively.

$$p\left(\frac{I}{I_x}\right) = \frac{\beta\left(\frac{\beta I}{I_x}\right)^{\beta-1}}{I_x \Gamma(\beta)} \exp\left(\frac{-\beta I}{I_x}\right) I > 0 \quad (7)$$

Using this assumption, we may say that the optical radiation is received as a plane wave. The irradiance fluctuation pdf is characterized by two variables and they are linked to the atmospheric conditions (Zabih Ghassemlooy, Popoola ve Leitgeb, 2007).

$$\alpha = \left[\exp\left(\frac{0.49\sigma_l^2}{\left(1+1.11\sigma_l^{12/5}\right)^{7/6}}\right) - 1\right]^{-1}$$
$$\beta = \left[\exp\left(\frac{0.51\sigma_l^2}{\left(1+0.69\sigma_l^{12/5}\right)^{5/6}}\right) - 1\right]^{-1} \quad (8)$$

While the SI. is given by

$$\sigma_N^2 = \exp\left[\frac{0.49\sigma_l^2}{\left(1+1.11\sigma_l^{12/5}\right)^{7/6}} + \frac{0.51\sigma_l^2}{\left(1+0.69\sigma_l^{12/5}\right)^{5/6}}\right] - 1 \quad (9)$$

To get the following gamma-gamma irradiance distribution function, the conditional probability p (I / I_x) is averaged across the statistical distribution of I_x given by the equation below.

$$p(I) = \int_0^\infty p\left(\frac{I}{I_x}\right) p(I_x)\mathrm{d}I_x$$
$$= \frac{2(\alpha\beta)^{(\alpha+\beta)/2}}{\Gamma(\alpha)\Gamma(\beta)} I^{(\alpha+\beta/2)-1} \mathrm{K}_{\alpha-\beta}(2\sqrt{\alpha\beta I})\mathrm{I} > 0 \quad (10)$$

Figure 2.2 depicts a plot of this distribution for three distinct turbulence regimes from weak to strong. The plot indicates that when the turbulence grows from mild to high, the distribution becomes widely available increasing the range of achievable irradiance values

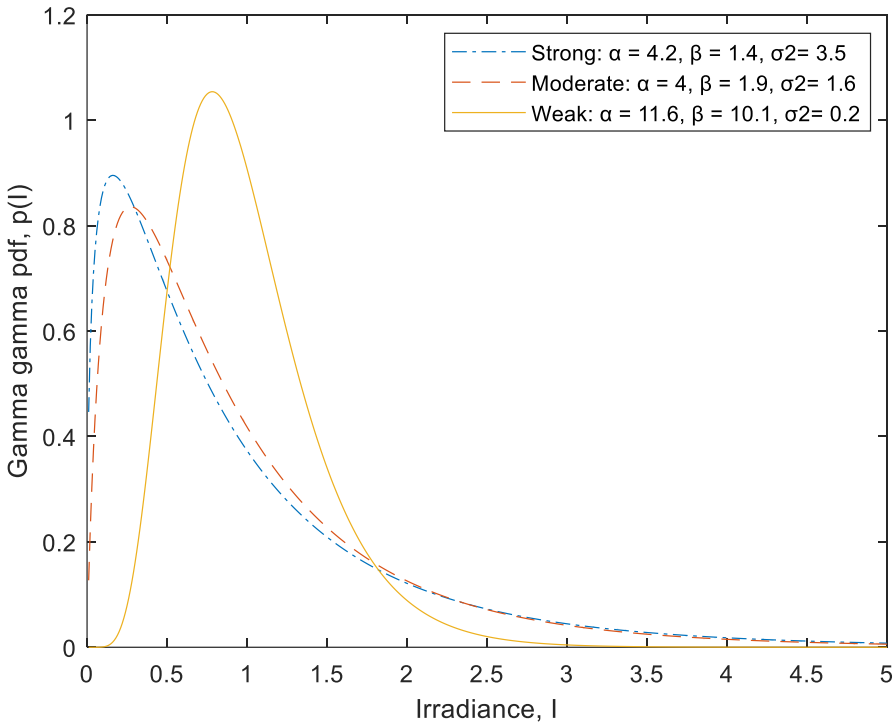

Figure 0.2. Gamma-Gamma model distribution

Figure 2.3 shows the values α and β in various systems of turbulence: mild, moderate-to-strong, and saturated regimes. In very mild turbulence, the number of small and large eddies is quite high, i.e. in (α >> 1) and (β >> 1) as illustrated in Figure 2.3. When the radiation differences increase (above = 0.2) and a system approaches the saturation region it starts decreasing dramatically and starts decreasing sharply, as shown in Fig. 2.3. As the saturation regime approaches and the focusing regime (moderate to strong) fades away, small-scale cell density gradually reduces to the transverse spatial coherence radius for optical waves. According to Figure ,2.3 the number of discrete refractive scatterers that may be employed efficiently increases with rising turbulence until it approaches saturation and is endless. Under these circumstances, the gamma-gamma distribution nears the negative exponential distribution.

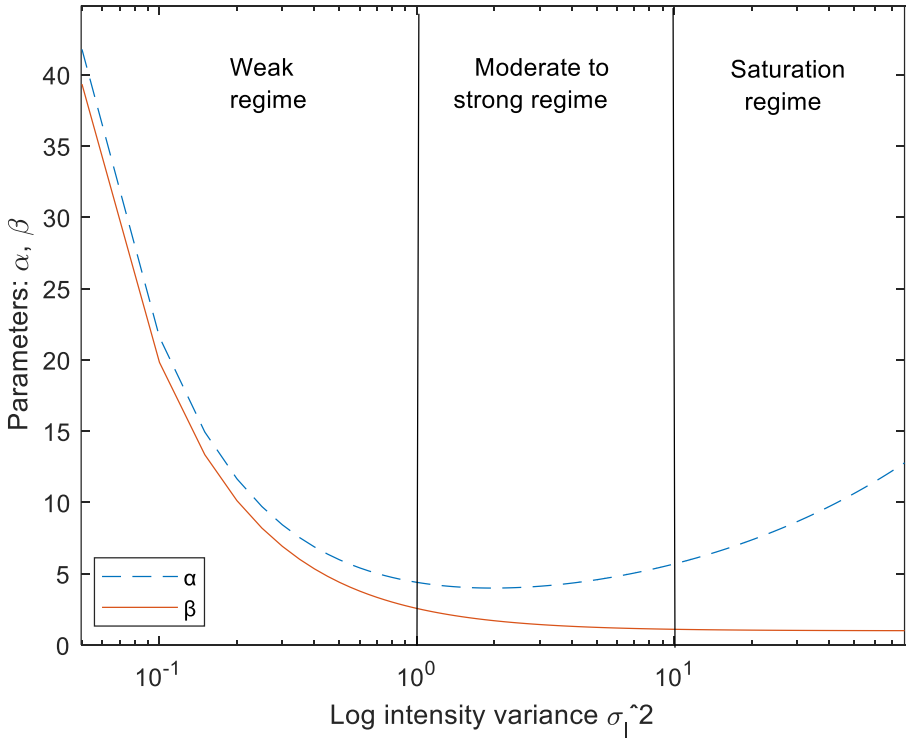

Figure 0.3. Parameters Of Various Turbulence

2.2.4 K-Distribution

The intensity fluctuation distribution in turbulent air for electromagnetic waves is often predicted using mathematical models. These models link discrete scattering locations into each turbulent medium electromagnetic wave irregularity. Radiation fields for electromagnetic waves are Gaussian, if there are enough discrete scattering points, radiation becomes not Gaussian fields in other turbulence channel models, where the statistics of the irradiance field are controlled by the negative exponential distribution. It is only possible to use this distribution model in the supersaturation regime since it demands the presence of a high number of scatters because of its widespread acceptance as a viable model for strong turbulence (Jakeman E. &., 1976). The K distribution provides intensity statistics for strong turbulence channels when (SI) is close to one and log intensity variance is between three and four. However, the theoretical and experimental parts of this model have a high degree of concordance (Jakeman E. &., 1976) .The K turbulence model is a combination of two distinct models exponential and gamma distributions. Research has shown how to obtain the K distribution from a modulation process in which the conditional irradiance is dictated by the negative exponential distribution(M Uysal ve Nouri, 2014).

$$f(I \mid \mu)(I \mid \mu) = \frac{1}{\mu}\exp\left(-\frac{1}{\mu}\right), I > 0 \qquad (21)$$

The gamma distribution is used to refer to mean irradiation μ.

$$f_{\mu}(\mu) = \frac{\alpha^{\alpha}\mu^{\alpha-1}}{\Gamma(\alpha)}\exp(-\alpha\mu), \mu > \mathbf{0} \qquad (32)$$

Since the number of discrete scatterers is proportional to the channel parameter, (α) indicates the gamma function. As an example, the irradiance distribution may be expressed as

$$\begin{aligned} f_I(I) &= \int_0^{\infty} f(I \mid \mu)(t \mid \mu) f_{\mu}(\mu) dI \\ &= \frac{2}{\Gamma(\alpha)}\alpha^{\frac{\alpha+1}{2}} I^{\frac{\alpha-1}{2}} \mathbf{K}_{\alpha-1}(2\sqrt{\alpha I}), I > 0 \end{aligned} \qquad (43)$$

where $\mathbf{K}_{\alpha}$**(.)** denotes the modified Bessel function (Gradshteyn, 2014). When α $\rightarrow \infty$ the gamma distribution approaches a K distribution and the delta function where the distribution shrinks to a negative exponential. However, the K distribution lacked closed-form numerical computations because of the difficulty in connecting mathematical properties with air turbulence. Uysal and Li approach was used to evaluate coded FSO systems to strong turbulence (Murat Uysal, Navidpour ve Li, 2004). In the presence of K-distributed turbulence fading, the BER performance of an FSO communication system is based on heterodynes (Jakeman E. &., 1976). FSO channel model with statistics that incorporate the effects of K distributed pointing errors as well as significant turbulence fading for the channel statistics (Jakeman E. &., 1978) .

$$f_h(h) = \frac{\alpha\gamma^2}{A_0\Gamma(\alpha)} G_{1,3}^{3,0}\left[\left(\frac{\alpha}{A_0}h \mid \begin{matrix}\gamma^2 \\ -1+\gamma^2, \alpha-1, 0\end{matrix}\right)\right] \qquad (54)$$

Where $A_0 = [\text{erf}(\upsilon)]^2, v = \frac{\sqrt{\pi}r}{\sqrt{2}}$, ω_z is the beam waist at distance z,$r = \omega_{\text{zeq}}/2\sigma_s$ and $\omega_{zeq}^2 = \frac{\omega_z^2\sqrt{\pi}\text{erf}(v)}{2v}\exp(-v^2)$

Here, erf(.) represents the error function, α parameter of the channel linked to the effective number of discrete scatters, and h represents the channel state(Farid ve Hranilovic, 2007).

The closed-form equation for BER of IM/DD with OOK in an FSO communication system using the K distribution is given as:

$$P_b(e) = \frac{2^{\alpha-3}\gamma^2}{\sqrt{\pi^3}\Gamma(\alpha)} G_{6,3}^{2,5}\left\{\frac{16P_t^2A_0^2}{\sigma_N^2\alpha^2} \mid \begin{matrix}\frac{2-\gamma^2}{2}, \frac{1-\alpha}{2}, \frac{2-\alpha}{2}, 0, 1 \\ \frac{0,1}{2}, \frac{-\gamma^2}{2}\end{matrix}\right\} \qquad (65)$$

Fig 2.4 displays the average BER in terms of transmitted optical power in dBm for various values of normalized beam width in increments of 5 (ω_z / r =5 to 25) with normalized jitter σ_s/ r = 0.1, noise standard deviation σ_N = 10 -7 A/Hz, and turbulence fading parameters α =2. When the received signal strength grows, narrow beam width

results in higher BER performance; nevertheless, the misalignment effect rises as the transmitter moves off line of sight in the direction of the receiver.

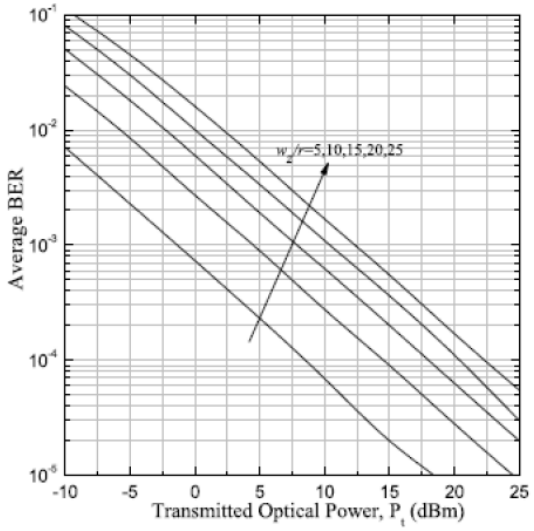

Figure 0.4. The Relationship between BER and Transmitter Power (Parikh, 2011)

2.3 System Parameters

It is necessary to identify the system based on numerous parameters, the most essential being the refractive index structure $C_n^2$and Scintillation Index (SI) coefficients that indicate the kind of air turbulence (mild, moderate, or intense) in the system.

2.3.1 Refractive Index Structure C_n^2

The spatial frequency is given by the refractive index structure parameter C_n^2 and the constants of refractive indices (C_n^2 in units of $m^{-2/3}$). Below are the values for various turbulence levels:

$$C_n^2 = \begin{cases} 10^{-17} m^{-2/3} & \text{for weak turbulence} \\ 10^{-15}\, m^{-2/3} & \text{for moderate turbulence} \\ 10^{-13}\, m^{-2/3} & \text{for strong turbulence} \end{cases} \quad (76)$$

The value is affected by, altitude, geographical location, and time during the day. The rate at which a horizontal line is stretched remains almost constant. As a result of temperature differences, the vertical/slant route shifts as the height varies (Yan, 2006).

Assume that C_n^2 is constant for applications involving horizontal propagation. However, a C_n^2 is necessary for the spread on a vertical or inclined path. Hufnagle-Valley model is employed by researchers most frequently with altitude function (h) (Yan, Zheng, Hu ve Xu, 2006).

$$C_n^2 = 0.00594\left(\frac{w}{27}\right)^2 (10^{-5}h)^{10}\exp\left(\frac{-h}{1000}\right) + 2.7\times 10^{-16}\exp\left(\frac{-h}{1500}\right) + A\exp\left(\frac{-h}{100}\right) \quad (87)$$

Where $A = C_n^2$ is a ground-level value $(1.7 * 10^{-14})$ and w is a root mean square (rms) wind speed, which is defined as:

$$w^2 = \left(\frac{1}{15}\right)\int_{5\times 10^3}^{2(\mathrm{k}]0^3} V^2(h)dh \quad (98)$$

$$V(h) = w_s h + w_g + 30\exp\left[-\left(\frac{h-9400}{4800}\right)^2\right] \quad (19)$$

Where $V(h)$ is the Bufton wind model's wind speed in meters per second as in the following :

.

$$w = \left[\frac{1}{15\times 10^3}\int_{3\times 10^3}^{20\times 10^5}\left\{w_r h + w_s + 30\exp\left[-\left(\frac{h-9400}{4800}\right)^2\right]\right\}^2 dh\right]^{1/2} (10)$$

Where h is the height, w_g is the ground wind speed, and w_s is the beam slew rate.

$$C_n^2 = 8.2\times 10^{-16}w^2\left(\frac{h}{10}\right)^{10}\exp(-h) + 2.7\times 10^{-16}\exp\left(\frac{-h}{1.5}\right) + \mathrm{A}\exp\left(\frac{-h}{0.1}\right) (11)$$

The most commonly used value for w is 21 m/s the value of the index of refraction structure parameter varies with altitude(Scholz ve diğerleri, 2016).

Temperature variations and the temperature structural constant (C_n^2) are the primary causes of horizontally propagating refractive index fluctuations. As a result, the C_n^2may have a considerable influence on the C_n^2 the following is the general case formula (Jeong, 2002) :

$$C_n^2 = \left(79 \times 10^{-6} \frac{P}{T^2}\right)^2 C_T^2 \qquad (12)$$

Where P the air is pressure (mB) and T is the air temperature (K). $C_T^2$is the proportionality constant in the inertial subrange version of the temperature structure-function $D_T(r)$ (Zhongming, 2018) (Qing ve diğerleri, 2017).

$$D_T(r) = \langle [T(\boldsymbol{x}) - T(\boldsymbol{x} + \boldsymbol{r})]^2 \rangle = C_T^2 r^{2/3}, l_0 \ll r \ll L_0 \qquad (13)$$

Where $\boldsymbol{x}$ and r denote the position vector, r is the magnitude of r , $\langle ... \rangle$represents the ensemble average and $l_0$and $L_0$are the inner and outer scales of the atmospheric turbulence, respectively

C_T^2 denotes a structural parameter. This inertial subrange of turbulence is the range from the tiny scale l_0 to the outer scale L_0 of turbulence. The tiny scale correlates to the eddy size, where viscous dissipation consumes the energy in the eddy more and more. The outer scale represents the biggest scale size for which eddies may still be considered isotropic. The structural parameter of temperature Kolmogorov spectrum for temperature changes can be calculated as below (Tatarski, 1961).

$$C_T^2 = \frac{\langle [T(r_2) - T(r_1)]^2 \rangle}{(r2 - r1_1)^{2/3}} \qquad (14)$$

Where T is the temperature (kelvin) and r is a distance (meters)

By utilizing the equation (21) of refractive index as a function of temperature and pressure with wavelength as a parameter, the refractive-index structure constant C_n^2 may be written in terms of the temperature structure constant C_T^2 equation (24). The impact of the temperature structure modulus C_T^2 on the refractive index $\boldsymbol{C_n^2}$ when the pressure is constant is clearly shown in figure 2.5. Where the temperature can have a significant impact on the amount of turbulence.

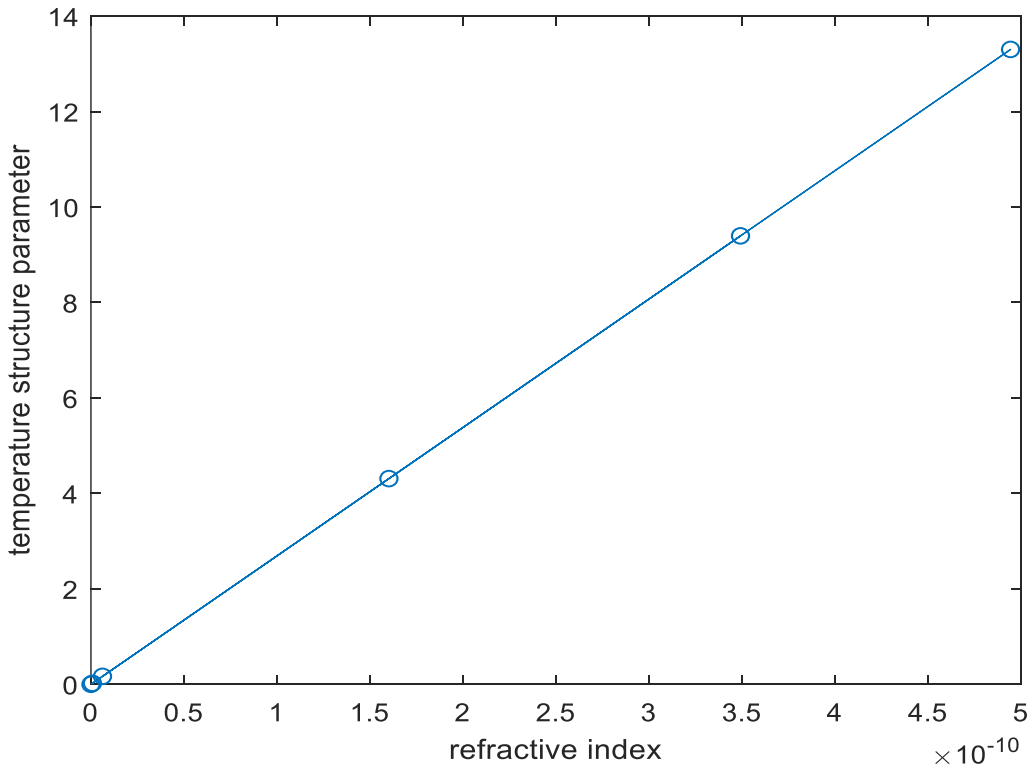

Figure 0.5.Relation between C_T^2 and C_n^2

2.3.2 Scintillation Index (SI)

Scintillation occurs because the index of refraction changes with temperature. Optical turbulence is another name for it. The Scintillation Index characterizes the received intensity variations, It is also known as "the degree of turbulence. Causes by the fading, beam parameters, distance of the spread, heights of a transmitter-receiver, and the fluctuations in the refractors' index. The SI is considered the primary parameter that describes turbulence strength (Zabih Ghassemlooy, Popoola ve Rajbhandari, 2019).

The light intensity fluctuations (so-called scintillation) of a horizontally propagated laser beam may be detected by the refractive index structure $\boldsymbol{C_n^2}$ and the inner scale of air turbulence because they may undergo a random shift when they are propagated by an inhomogeneous medium. These results in fluctuations in light intensity on average there are fluctuations in the output intensity owing to turbulence. SI, a parameter for turbulence strength, is defined as (Kerr, 1972),(Kerr, 1972):

$$\sigma_{SI}^2 = \frac{\sigma_I^2}{E[I]^2} = \frac{E[I^2]}{E[I]^2} - \mathbf{1} \qquad (15)$$

Where I the intensity of the optical field is received after passage in the turbulent medium. It can evaluate the turbulence type depending on the Rytov variance values σ_R^2 :

$$\sigma_R^2 = 1.23 C_n^2 \mathrm{k}^{7/6} \mathrm{L}^{11/6} \qquad (16)$$

Where C_n^2 is the index of refraction structure parameter, k is the optical wave number defined as $2\pi/\lambda$, λ is the wavelength of the laser beam and L is the length between transmitter and receiver. The following are the several ranges of σ_R^2values that define the various turbulence conditions:

$$\begin{aligned} &\sigma_R^2 < 1 \text{ (weak fluctuations)} \\ &\sigma_R^2 \approx 1 \text{ (moderate fluctuation)} \\ &\sigma_R^2 > 1 \text{ (strong fluctuations)} \\ &\sigma_R^2 \gg> 1, \sigma_R^2 \to \infty \text{ (saturation regime)} \end{aligned} \quad (17)$$

In terms of system efficiency, the scintillation index is a critical factor. Fig. 2.6 depicts the influence of the scintillation index concerning different average signal count values. At an average signal intensity of 140 photons, a scintillation index of 0.2 may be detected. However, when the scintillation index is 0.45, the average signal rises to 260 photons. If air turbulence rises, the signal level should be raised to maintain system functions(Kiasaleh, 2005).

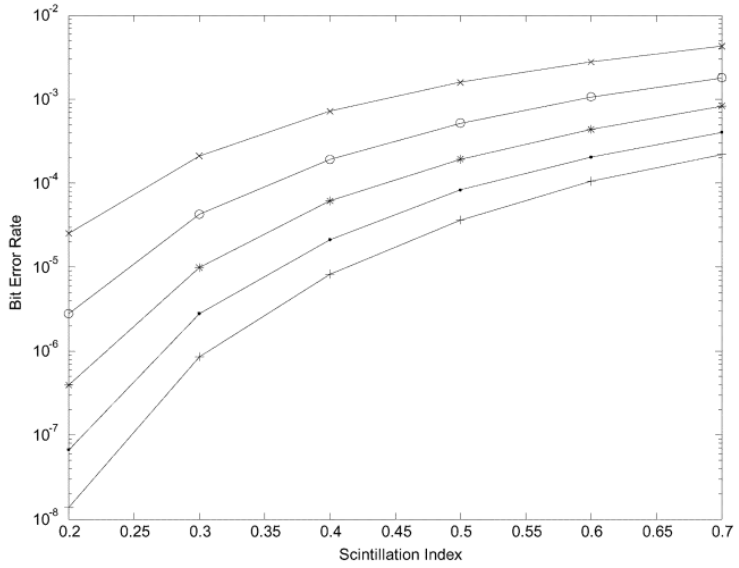

Figure 0.6. Scintillation & BER (Parikh ve Jain, 2011)

2.4 System Variables

The link margin (M_{link}) is an important quality metric in FSO links, it is composed of transmitter power, receiver sensitivity, divergence angle, and atmospheric attenuation caused by the atmospheric channel. The specifications of free-space optical data connections are determined by the medium, the atmosphere, through which they travel. The cause of transmission degradation is the combination of geometric and atmospheric elements. The overall loss can measure optical power according to the following (Wilfert, 2010):

$$M_{link}(dB) = P_e + |S_r| - Att_{geo}(dB) - Att_{mol} - P_{tot} \quad (18)$$

- P_e is the transmitter's power factor (dBm)

- S_r is the recipient's responsiveness (dBm)

-Att_{geo}The geometrical loss of a link(dB)

-Att_{mol} Loss at the molecules(dB)

- P_{tot} Other system loss (dB)

2.4.1 Geometrical Attenuations

Because of the narrow receiver capture area, the light beam diverges as it travels a long way, consuming relatively little power. This issue corresponds to attenuation due to geometry (GA), where the attenuation can be expressed as:

$$Att_{geo} = 20\log(\mathrm{R}\theta/s_{\mathrm{capture}})\mathrm{dB} \quad (19)$$

Where θ is a ray divergence, R distance in kilometers between the transmitter and receiver, and s_{capture} is the receiver's capture area (Sari ve Ozek, 2011).

2.4.2 Attenuation at the Molecules

There is an inverse proportional relationship between wavelength and molecular attenuation. As shown in the table 2.1 (Sari, 2011) (Chabane, Al Naboulsi, Sizun ve Bouchet, 2004). As a result, it is possible to infer that molecular attenuation would have less of an impact on FSO output than additional variables affecting attenuation.

Table 0.1. Molecular attenuation values

Wavelength	Attributes
550μm	0.13 dB
690μm	0.01 dB
850μm	0.41 dB
1550μm	0.01 dB

2.5 Link Losses

Outdoor FSO systems provide a high data rate, a wide range of connections, and a high degree of system reliability. Like those of RF systems, are significantly influenced and constrained by the atmosphere. Particles in the atmosphere including rain, aerosols, gases, fog, and temperature all cause significant optical attenuation. Fog is by far the most serious of these issues. The attenuation of FSO devices ranges from a few dB per kilometer in a clear weather environment to more than 200 dB per kilometer in heavy fog (Chabane, 2004). The availability of the FSO connection is limited due to significant attenuation caused by the dense fog situation, it may reach 500m in range(Willebrand ve Ghuman, 2002). Dense (thick) fog, on the other hand, is more confined, lasting for a short time and appearing in a few areas. Irradiance and phase fluctuation are two further factors that contribute to the performance of FSO deterioration in a clear environment. The connection range might be as much as 5–10 kilometers in clear air conditions. However, fading of the optical beam traveling the atmospheric channel may be affected by temporal oscillations in temperature, pressure, and air humidity, which may lead to inconsistencies in the surrounding air pockets. A line-of-sight RF (microwave and millimeter) channel's loss processes are essentially similar to those of an FSO. But the fading level is greater. Optical signals traveling via a free space channel are extremely sensitive to weather conditions like

fog, rain, and so forth. Where particulate and molecular components of the atmosphere interact with optical radiation and extinguish some of the photons as they pass through the atmospheric channel. The Beer-Lambert law describes the transmission of an optical field through the atmosphere as a function of propagation distance (Bouchet O. E., 2008).

2.5.1 Fog and Visibility Attenuation

The sight near the ground is reduced due to fog particles. The meteorological definition of the fog is when visibility is reduced to less than one kilometer. Fog of various kinds causes varying degrees of optical loss this is mostly related to fog distribution particle size and particle location. Fog arises when the air is sufficiently cold and moist. Particle sizes range from 1 to 3 μm, and liquid water concentrations range from 0.01 to 0.1 g/m³. Convection occurs more often at night and near the end of the day. While it has no impact on longer wavelengths (the 1st and 2nd transmission windows)(Al Naboulsi, Sizun ve de Fornel, 2004).

Table 2.2 depicts the association between various atmospheric weather and the visibility range.

Table 0.2. International visibility code(Z Ghassemlooy ve diğerleri, y.y.)

International Visibility Code					
Atmospheric Conditions	**Weather Constituents (mm/h)**			**Visibility (m)**	**Attenuation (dB/km)**
Dense fog				50	315
Thick fog				200	75
Moderate fog				500	28.9
Light fog	Snow	Storm	100	770	18.3
Very light fog				1000	13.8
		Strong rain	25	1900	6.9
Light mist				2000	6.6
		Average rain	12.5	2800	4.6
Very light mist				4000	3.1
		Light rain	2.5	5900	2
				10,000	1.1
Clear air		Drizzle	0.25	18,100	0.6
				20,000	0.54
Very clear air				23,000	0.47
				50,000	0.19

Both Kim and Kruse's models are often used to evaluate fog attenuation for the attenuation coefficient given by: (Kruse, 1962) (Bouchet O. M., 2005)

$$\alpha_{\text{fog}} = \frac{10\log \text{V\%}}{\text{V(km)}} \left[\frac{\lambda}{\lambda_o}\right]^{-q} \quad (20)$$

Here, V(km) denotes the visibility range, V% denotes the transmission of air drops as a percentage of clear sky, λ denotes the wavelength in nanometres, λ_o is the visibility range reference, which is set to 550 nanometres, and q denotes the scattering size distribution coefficient (Kruse ve Laurence, 1962). In the investigation, the parameter " q" provided by the Kruse model may be derived by:

$$q = \begin{cases} 1.6, & \text{if V} > 50\text{km} \\ 1.3, & \text{if 6Km} < \text{V} < 50\text{km} \\ 0.16\text{V} + 1.344, & \text{if 1Km} < \text{V} < 6\text{km} \\ \text{V} - 05, & \text{if 0.5Km} < \text{V} < 1\text{km} \\ 0, & \text{if V} < 0.5\text{km}. \end{cases} \quad (21)$$

According to the Kruse model in equation (31), attenuation is less of an issue for longer wavelengths. Fig. 2.7 shows that 1550 nm will have a reduced attenuation due to shorter wavelengths. However, in the event of severe fog, i.e., limited visibility range circumstances, Kim's model, as in equation (31), eliminates the reliance on wavelengths for optical attenuation.

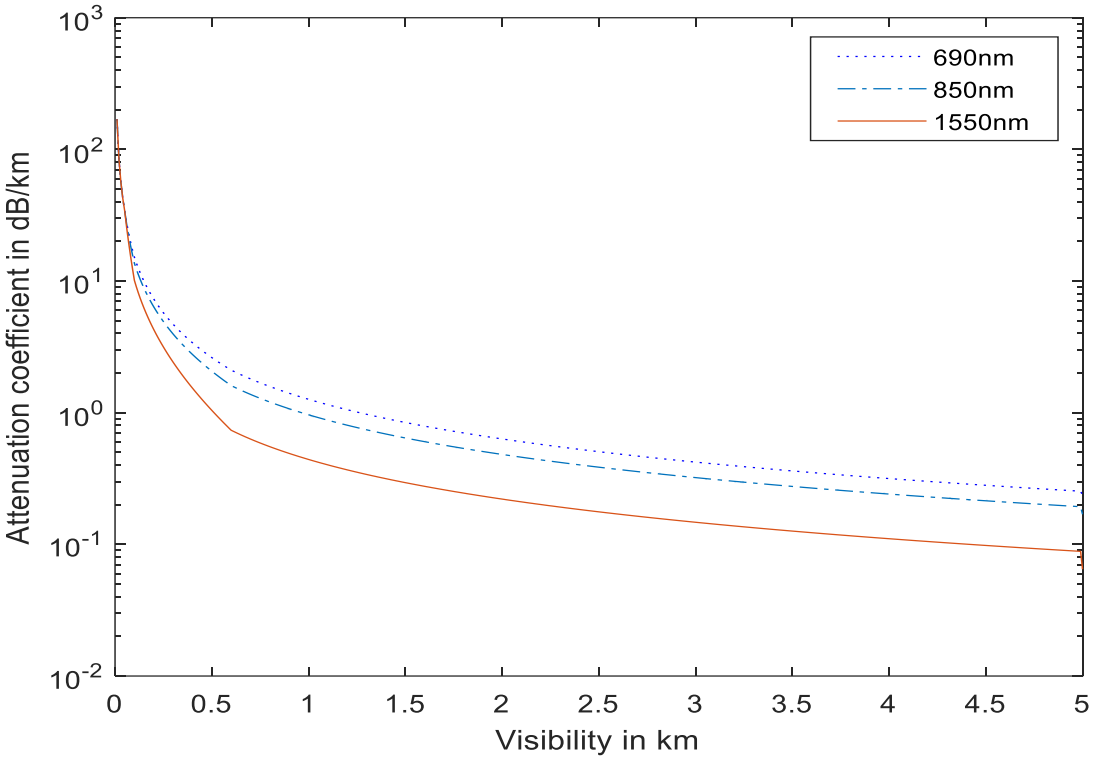

Figure 0.7. Attenuation coefficient of visibility

2.5.2 Rain Attenuation

A rain attenuation factor is considered in the FSO channel and expressed in terms of attenuation per unit length (Zhang, 1999). The rain attenuation effect is used to measure the impact of rain on data transmission via FSO connections. Rain has a lower attenuation of optical beams than clouds. In Moderately resistant optical systems, the connection margin is at least 25 dB. Raindrops have a larger wavelength by several orders of magnitude than the optical signal. Rain's attenuation is determined by depending on the size of raindrops The following relationship can be used to determine specific rain attenuation (Rashidi, He ve Chen, 2017):

$$A = kR^{a} \qquad (22)$$

Where A denotes the attenuation (dB/Km) caused by rain, a, and k, therefore, are power-law parameters, and R denotes the rate of rainfall in mm/hr.

Equation(32) describes the general case of the calculation of the attenuation by the effect of the rainfall rate. As seen in figure 2.8, the rate of attenuation rises per dB/km as the rainfall rate increases.

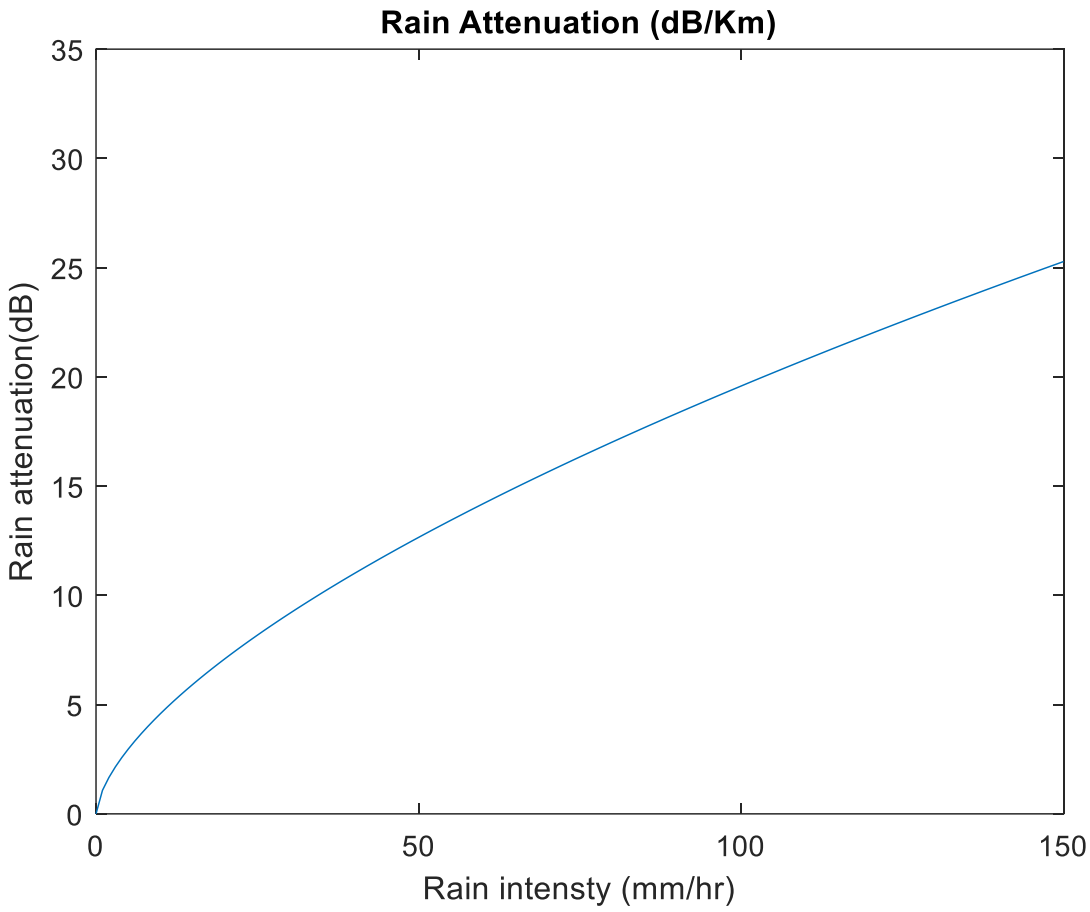

Figure 0.8. Relationship between the attenuation and rain intensity

Table 2.3 specifies the parameters' values (k, a) depending on the classification of rain type and the rainfall rate. When it rains, the loss of optical power is unaffected by wavelength but an established experimental model for rain relies on visibility (Awan, 2009).

$$\alpha_{Rain} = \frac{2.9}{V} \tag{23}$$

Table 0.3. Classify the rain based on the amount of rainfall (Soni, 2018)

Rainfall Rate	Value of $R\ mm/hr$	k	a
cold and rainy or a gentle drizzle	$(R < 3.8)$	0.509	0.63
moderate rain	$(3.8 < R < 7.6$	0.319	0.63
Substantial Rainfall (storm)	$(R < 7.6)$	0.163	0.63

2.5.3 Snow Attenuation

Snow has an impact on the FSO connection's performance. Snow is essentially defined as the freezing of precipitated water. The attenuation induced by snow differs according to location and is dependent on the weather condition of a specific location. The physical properties of snow are the primary cause of the deterioration of optical connections in free space. The attenuation resulted from snow $\alpha_{S_{\text{now}}}$ in dB/km is divided into two categories: wet and dry snow attenuation, it can be found using the equation (34).

$$\alpha_{S_{\text{now}}} = aS^b \qquad (24)$$

Where S is the snowfall rate (in millimeters per hour [mm/hr]), and a , b are parameters that depend on snow type, their values are specified in the table (2.4) (Muhammad, 2005).

Table 0.4. The values of parameters (a, b) based on the snow type (Muhammad, Kohldorfer ve Leitgeb, 2005)

Type of Snow	a	b
Wet	$1.023 \times 10^{-4}\lambda + 3.7855466$	1.38
Dry	$5.42 \times 10^{-5}\lambda + 5.4958776$	0.72

Figure 2.9 clearly shows that the attenuation in the case of wet snow is more than that of dry snow, the higher the snowfall rate.

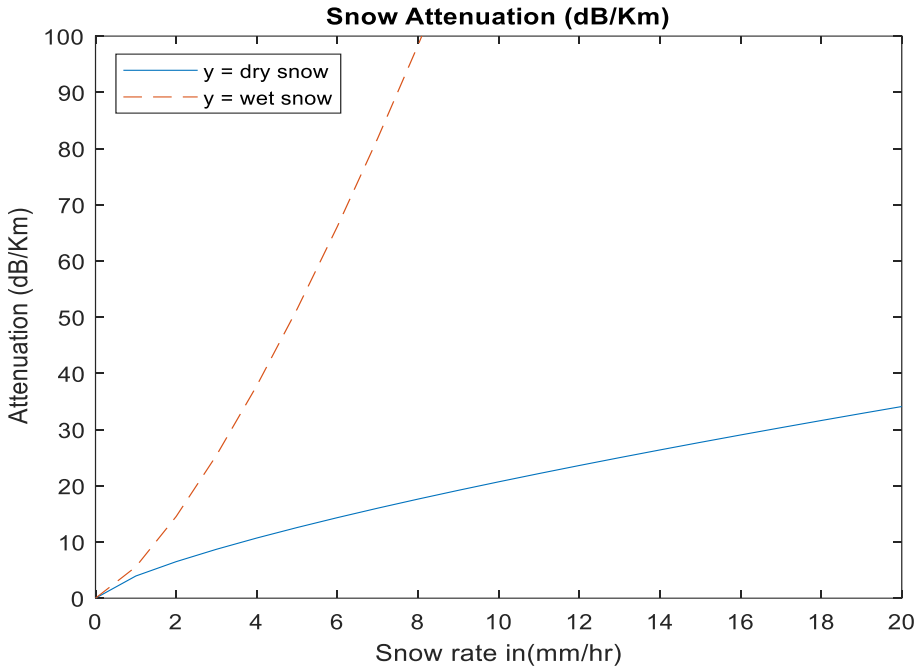

Figure 0.9. Relationship between attenuation and snow rate

Because of the significantly bigger droplet size, snow attenuation may be much greater than rain attenuation. According to (Manohar, 2016) the attenuation for snow dependent on V the visibility range is:

$$\alpha_{\text{Snow}} = \frac{58}{V} \qquad (25)$$

2.5.4 Attenuation of Haze

The Beer-Lambert law is used to determine the attenuation of the atmosphere caused by haze.

$$\tau = e^{-\sigma l} \quad (26)$$

Where l is the measurement's propagation distance, and "σ " is the specific attenuation per length unit it can be computed using the following equation:

$$\sigma \cong \frac{3.912}{V}\left(\frac{\lambda}{550}\right)^{-q} \quad (27)$$

Where V is the visibility in (km) and q is the scattering particles' size distribution, its values are given below (Niaz, 2019).

$$q = \begin{cases} 1.6, & V > 50\text{km} \\ 1.3, & 6\text{Km} < V < 50\text{km} \\ 0.585V^{\frac{1}{3}}, & V < 6\text{km} \end{cases} \quad (28)$$

Haze and visibility attenuations over distance in dB/Km can be expressed in figure 2.10.

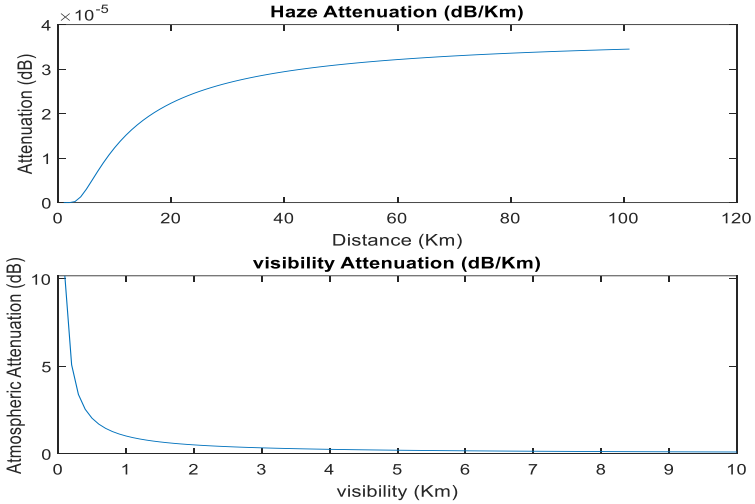

Figure 0.10. Haze and visibility attenuation

Table 2.5 shows the relationship of wavelength to atmospheric attenuation. Where the value of the attenuation decreases with increasing wavelength as a function of visibility.

Table 0.5. Atmospheric attenuation (Bouchet ve diğerleri, y.y.)

Visibility (km)	**Attenuation dB/km**		**Status**
	785 nm	**1550 nm**	
0.05	340	340	Fog
0.2	85	85	
0.5	34	34	
1	14	10	
2	7	4	Haze
4	3	2	
10	1	0.4	Clear
23	0.5	0.2	

CHAPTER THREE

THE CHARACTERIZATION OF AN OPTICAL CHANNEL IN AN ADVERSITY ENVIRONMENT

3.1 Introduction

As a city with a diverse climate that includes responses to weather conditions (heat, rain, snow, fog), this chapter will study and analyze actual data from Istanbul. To find out the appropriate model to represent this type of system and the most effective dilutions in creating FSO channels, calculate the system quality parameters. FSO channels may be affected by a broad variety of elements in the surrounding environment. As a result, there is a significant requirement to assess the dependability of weather conditions on FSO channels .The mathematical model of attenuation coefficients is based on measurements of the 1550 nm wavelength to explain the relationship between temperature, reflective index, attenuations, scintillation, and wavelength. The data were collected in Istanbul for the yearly rate (2021) of snowfall and rainfall during the winter season. To further understand how the weather affects FSO connections in general, research was conducted using a variety of various parameters, such as air attenuation, molecular attenuation values, geometric attenuation, and haze. In figure 3.1 Europe and Asia are divided by the Bosphorus Strait, a 10-kilometer-long canal that links the Black and Marmara seas, where the FSO link's communication route is both affordable and easy to set up.

Figure 0.1. Bosphorus Strait (Barnett, 2018)

The recommended link for the study is to connect the two sides with a distance less than 2.5 km, as shown in Figure 3.2 between the districts of Fatih European/Istanbul and Kadikoy Asian/Istanbul.

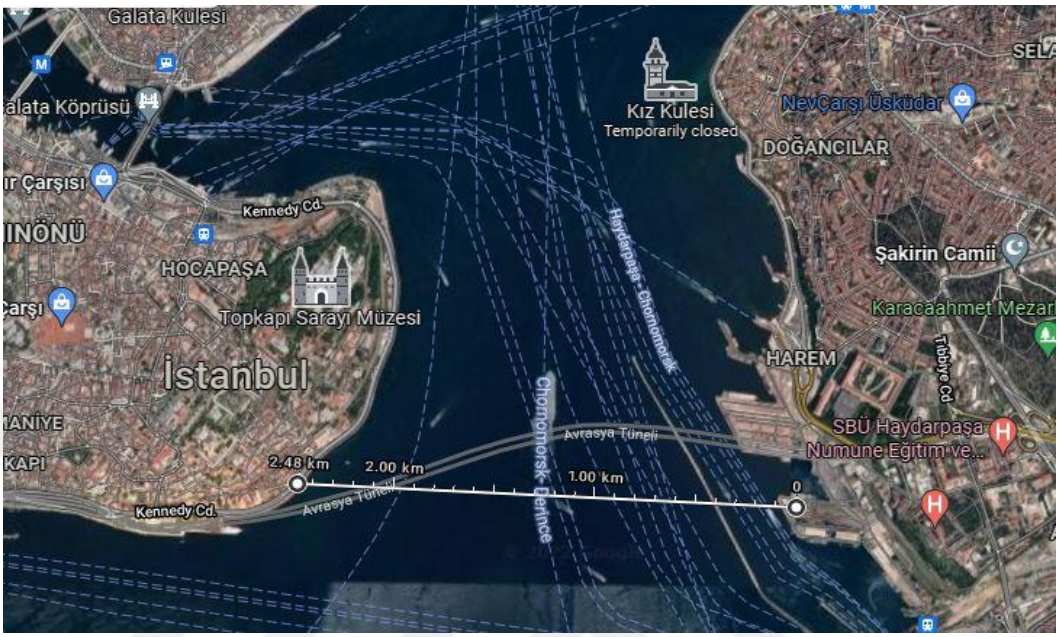

Figure 0.2. The recommended FSO link(“www.google.com/maps/”, y.y.)

3.2 Meteorological Analysis

To study any model, we need weather data to know the impact of weather factors on the communication channel. In this chapter, the real data for the districts of Fatih and Kadikoy are discussed according to the meteorological readings of Istanbul over the months of the year. The climatic diversity in Istanbul provides a suitable environment to study all the factors that affect the FSO. Furthermore, the meteorological data of the transmitter and receiver area will be collected to achieve the link region analysis that is most accurate to facilitate the study of the model.

3.2.1 Fatih

Fatih district is located in the European part of Istanbul (Latitude: 41.0037102145184°, Longitude: 28.98199284848689 °). Figure 3.3 displays the highs and lows of weather temperatures during different periods of the year. Fig.3.3 displays monthly measurements of atmospheric pressure; the lowest was measured in the middle of the year in July, while the highest was recorded at the end of the year in December.

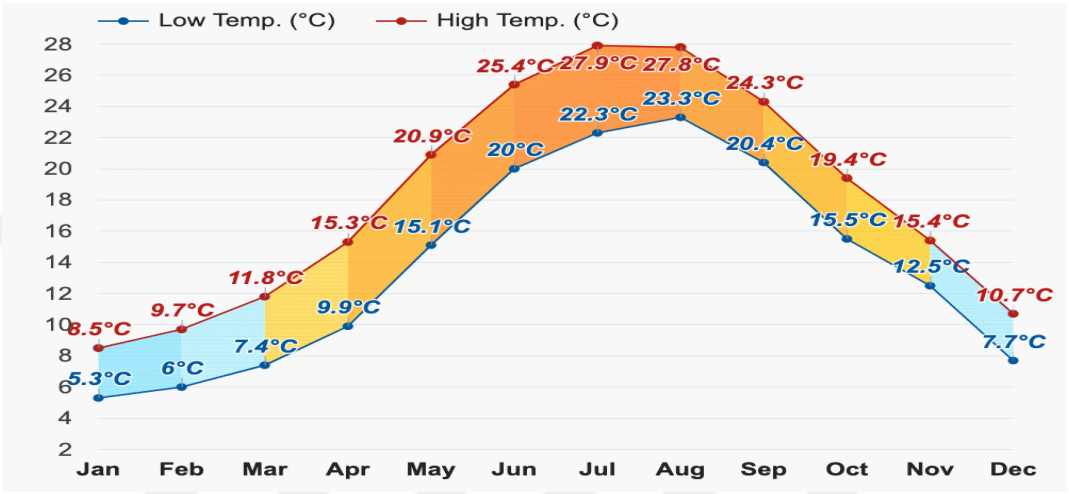

Figure 0.3. Temperature – Fatih (“www.weather-atlas.com-istanbul”, y.y.)

Fig. 3.4 displays the year's highest and lowest wind speeds, whereas August displays the highest wind speed, while May has the lowest wind speeds of the year.

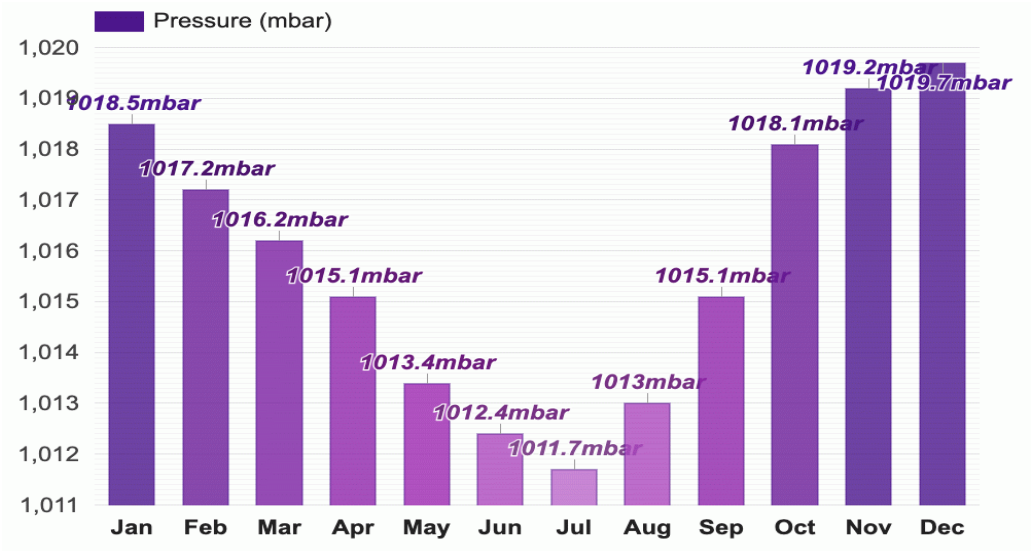

Figure 0.4. Pressure-Fatih(“www.weather-atlas.com-istanbul”, y.y.)

Fig. 3.5 displays the year's highest and lowest wind speeds, whereas August displays the highest wind speed, while May has the lowest wind speeds of the year

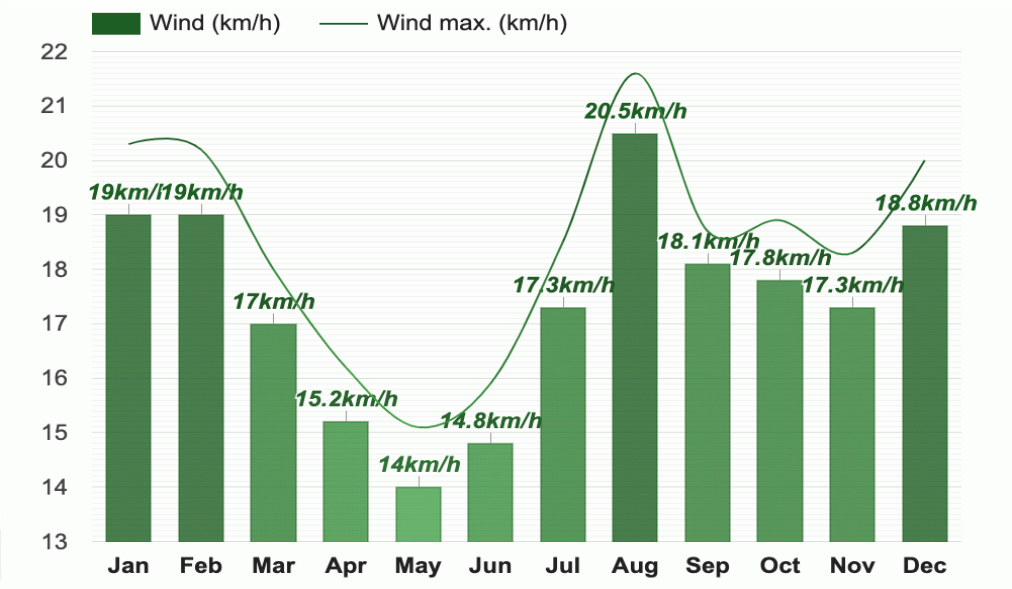

Figure 0.5. Wind speed - Fatih(“www.weather-atlas.com-istanbul”, y.y.)

Fig. 3.6 illustrates the month's rainfall, with the heaviest in December and the lightest in August.

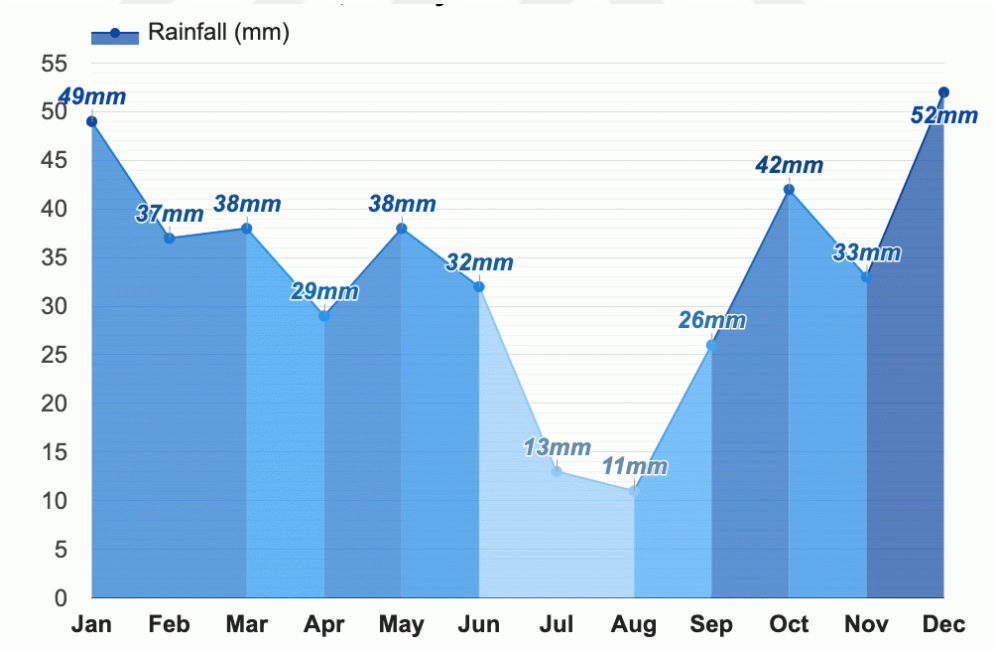

Figure 0.6. Rainfall-Fatih (“www.weather-atlas.com-istanbul”, y.y.)

Fig. 3.7 shows the snowfall rate in a year. It starts at the end of the year and peaks in January next year. After that, it keeps declining until it reaches a complete stop at the end of March.

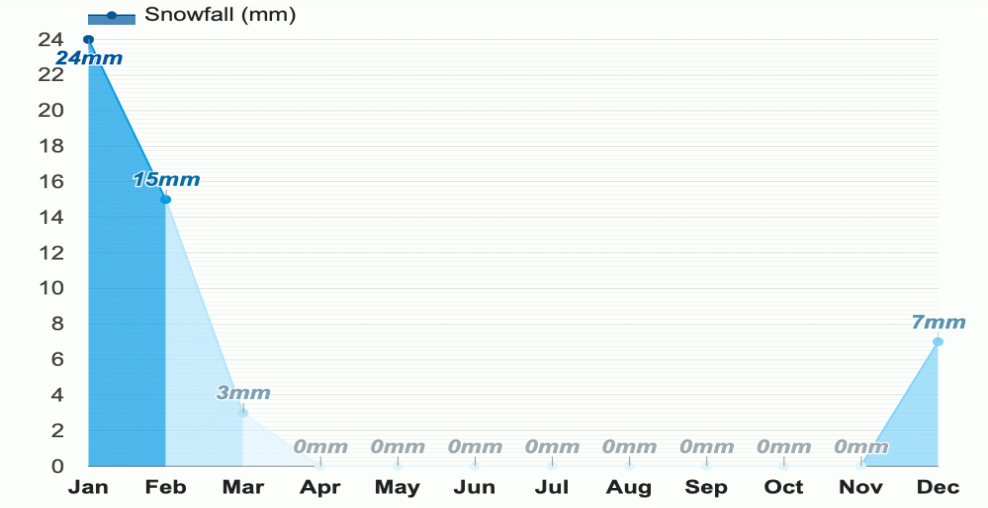

Figure 0.7. Snowfall-Fatih (“www.weather-atlas.com-istanbul”, y.y.)

Figure 3.8 shows that the average visibility is constant for the months from March to December. While it is at a lower rate for January and February.

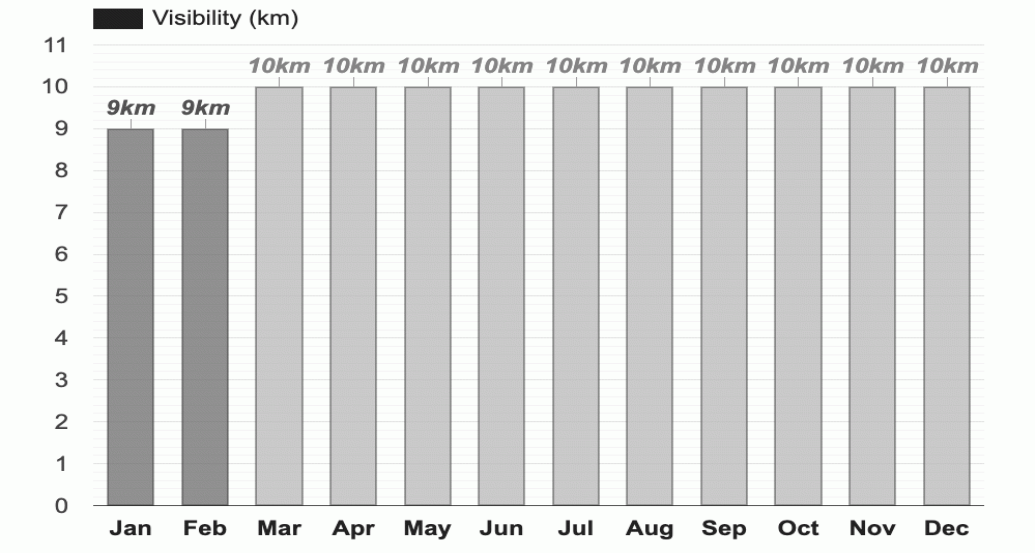

Figure 0.8. Visibility-Fatih (“www.weather-atlas.com-istanbul”, y.y.)

3.2.2 Kadikoy

Kadikoy is located in the Asian part of Istanbul in the coordinates (Latitude: 41.00234995498352°,Longitude:29.011261113094402°)(“www.google.com/maps/ ”, y.y.). Fig. 3.9 shows Kadikoy’s average low and high temperatures over the year.

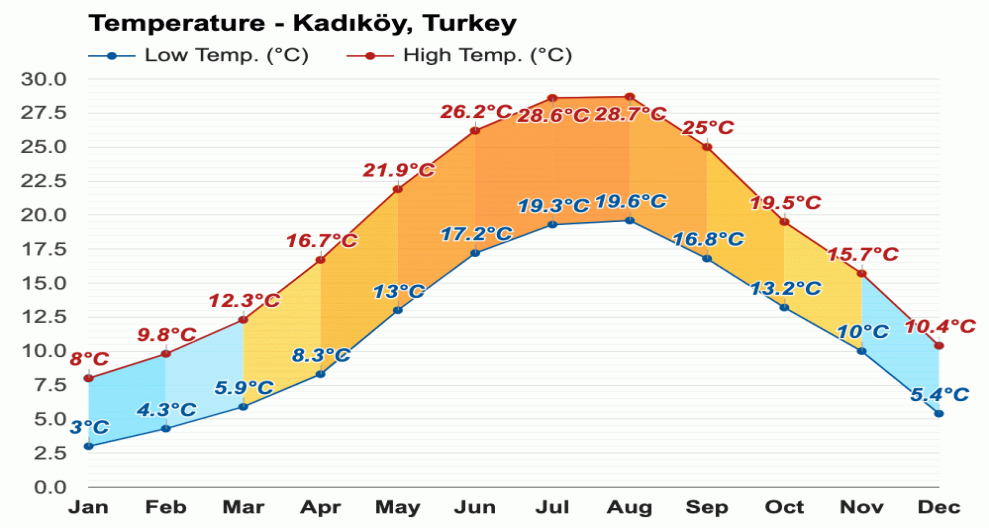

Figure 0.9. Temperature- Kadikoy(“www.weather-kadikoy”, y.y.)

Fig. 3.10: Kadikoy's recorded atmospheric pressure throughout the year, the highest was in December, while the lowest was in July.

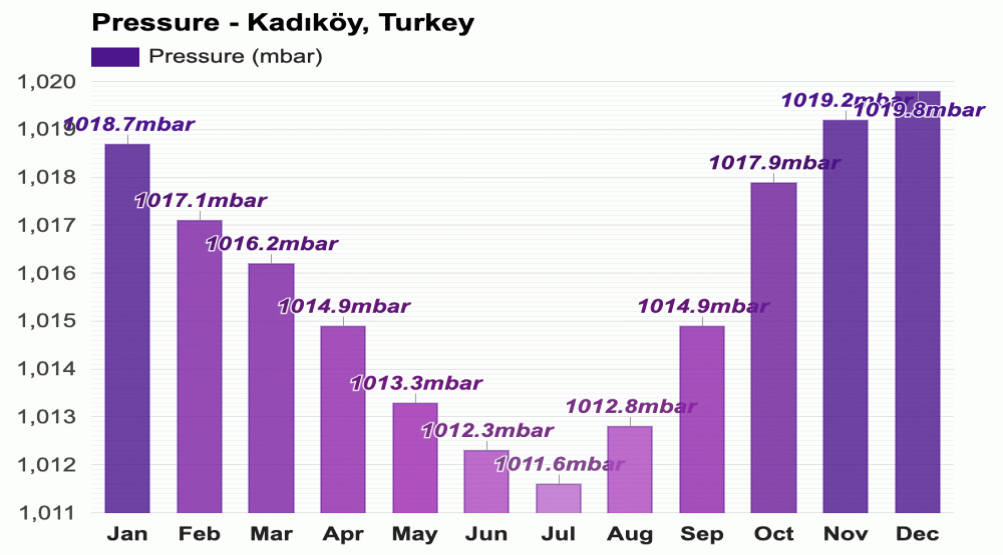

Figure 0.20. Pressure - Kadikoy(“www.weather-kadikoy”, y.y.)

In figure. 3.11, the greatest and lowest wind speeds for each month in Kadikoy, August showed the fastest, while May displayed the slowest wind speeds.

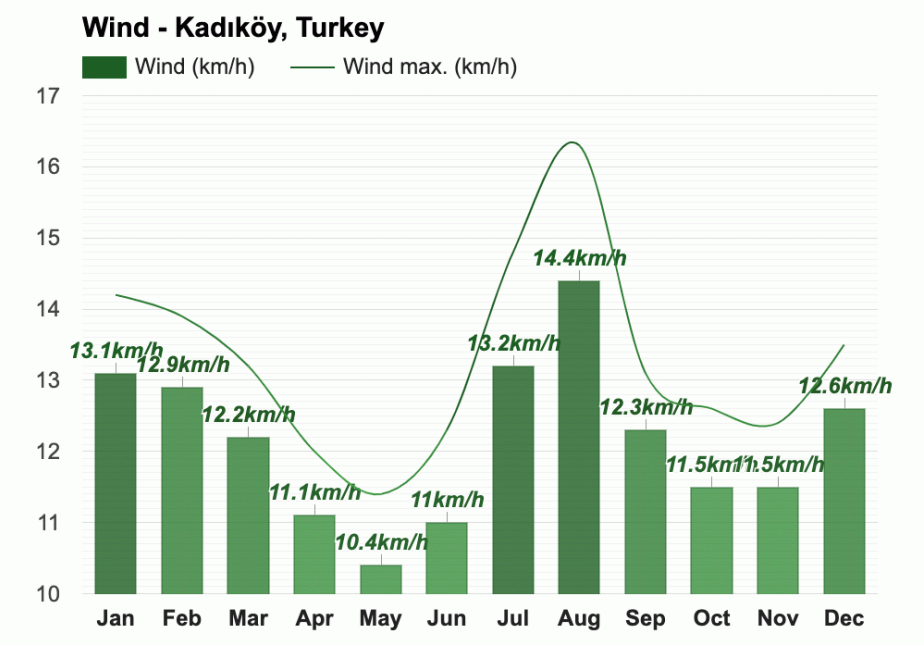

Figure 0.31. Wind – Kadikoy(“www.weather-kadikoy”, y.y.)

Figure 3.12 shows the annual snowfall rate in Kadikoy. Where the highest rate was in January and the lowest rate was in the month of March.

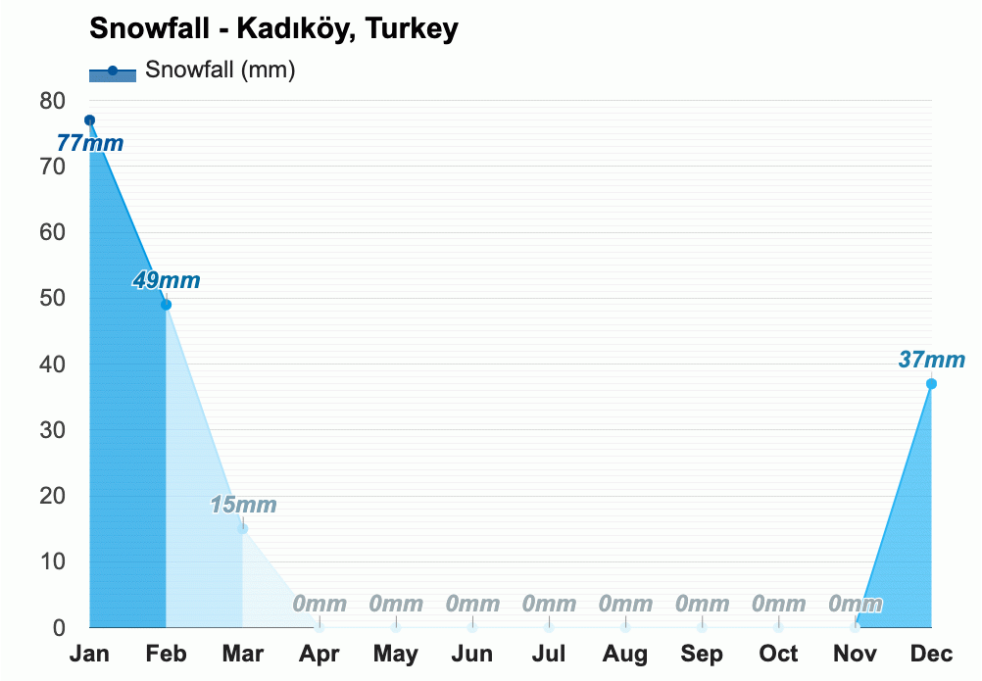

Figure 0.42. Snowfall-Kadikoy (“www.weather-kadikoy”, y.y.)

Figure 3.13 shows the annual rainfall in Kadikoy, the highest rate was in December, and the lowest was in August.

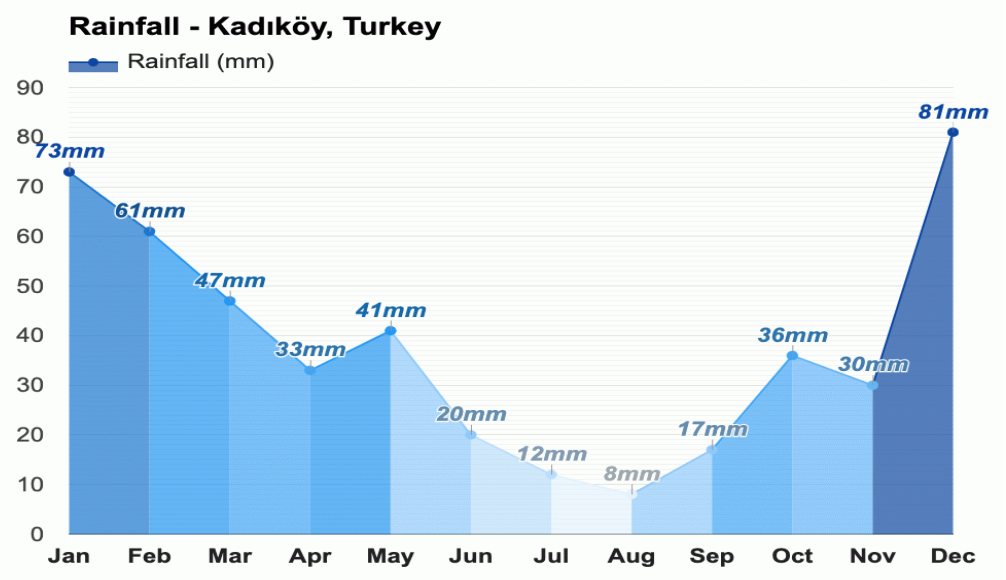

Figure 0.53. Rainfall -Kadikoy("www.weather-kadikoy", y.y.)

Figure 3.14 shows the annual average visibility in Kadikoy, over the visibility was very high throughout the year.

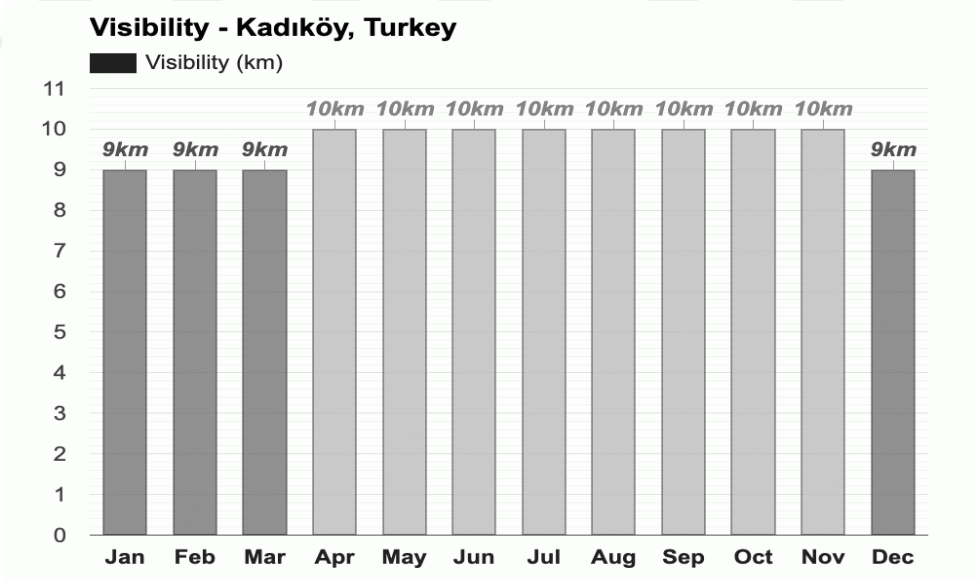

Figure 0.64. Visibility-Kadikoy("www.weather-kadikoy", y.y.)

3.3 Data Analysis

The data obtained from the planned linking location will be analyzed for patterns in an application coded in the Matlab environment. The program was written in Matlab language and has an intuitive graphical user interface (GUI) shown in Figure 3.15, where models, atmospheric, and geometry attenuations are all calculated using the equations for the system discussed in the previous chapter. Using values entered in the applications' input textboxes which are:

- Distance in meters
- wavelength in nanometers
- receiving lens area in centimeters
- transmitting power in decibel milliwatts
- receiving sensitivity in decibel milliwatts

Figure 0.75. The data entry section of the GUI

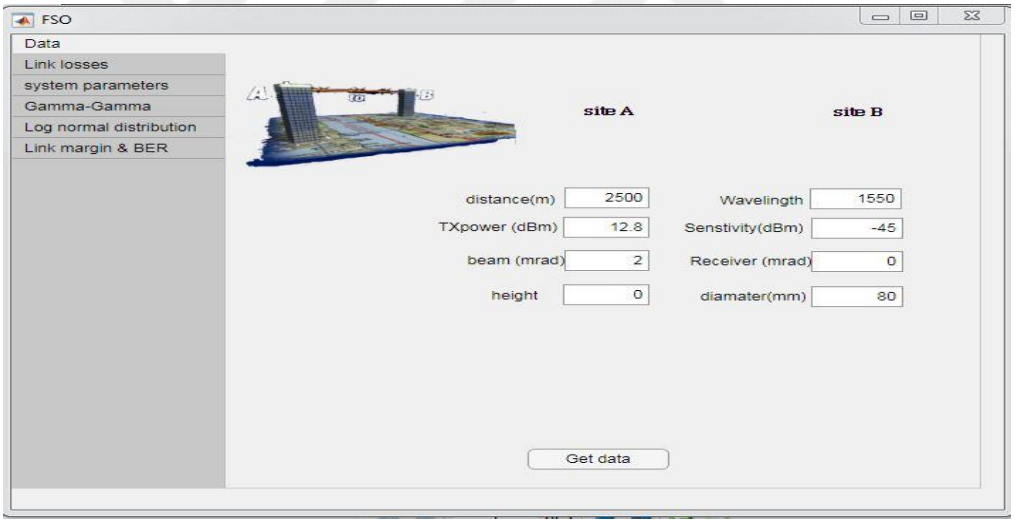

For the recommended FSO link, the inputs were: (2500 m) as the distance, the wavelength set as (1550nm), transmitting power rated at (12.8 dBm), the receiving sensitivity measures at (-45 dBm), and the area of the receiving lens was (80 cm). With inputs taken into account, the application will determine how all of the different factors and losses can affect a connection's performance.

3.4 System Parameters Of The Link

The average values of the data were placed into the system's coefficients (C_T^2, C_n^2, SI). The system's characteristics were computed based on the data obtained from Figures (18-20 and 24-26), which include annual data for:

- maximum and minimum temperatures in Celsius
- atmospheric pressure in millibar
- wind speed in kilometers per hour

The software shown in Figure 3.16, computed the results for both locations, based on equations 22, 24, and 26 sequentially. The proper model for analyzing the recommended link may be determined by identifying the types of disturbances (mild, moderate, and strong).

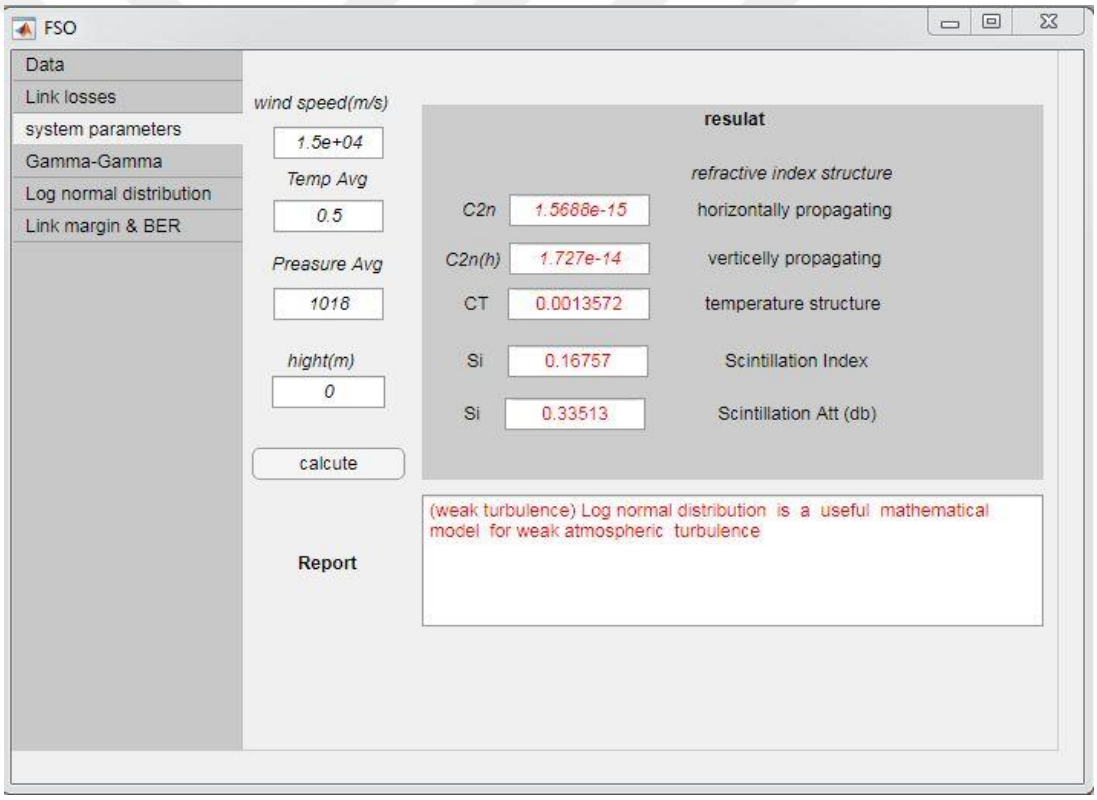

Figure 0.86. Calculation of parameters

Table 3.1 shows various values that were calculated for the maximum and minimum temperatures, with an average air pressure of (1016 mb) and an average wind speed of (15000m\s).

Table 0.1. System Parameters of the Link

Months	C_T^2/low	C_T^2/HI	C_n^2/low	C_n^2/hi	SI /low	SI /hi
Jan	0.028719	0.0013572	3.23E-14	1.56E-15	3.4376	0.16678
Feb	0.015689	0.00542	1.78E-14	6.28E-17	1.8945	0.00671
Mar	0.0122149	0.0013572	1.39E-14	1.58E-15	1.4792	0.16678
Apr	0.0138979	0.010641	1.58E-14	1.21E-14	1.6806	0.010641
May	0.023941	0.0054288	2.70E-14	6.20E-15	2.8741	0.66225
Jun	0.042562	0.0034745	4.76E-14	3.98E-15	5.0578	0.42508
Jul	0.04886	0.0026601	5.45E-14	3.11E-15	5.7894	0.32593
Aug	0.074321	0.0043974	8.20E-14	5.16E-15	8.7175	0.53721
Sep	0.070358	0.0026601	7.77E-14	3.11E-15	8.2646	0.32593
Oct	0.028719	5.43E-05	3.23E-14	6.30E-17	3.4376	0.00671
Nov	0.03393	0.0004886	3.81E-14	5.69E-16	4.0497	0.060215
Dec	0.028719	0.0004886	3.23E-14	5.64E-16	3.4376	0.060215
Mean AVG	0.032587	0.0012249	3.66E-14	1.43E-15	3.8921	0.15268

The results that appear for C_n^2 rates can be classified according to Equation (16) between moderate to weak for maximum temperature. It is possible to classify atmospheric turbulence through SI values, according to the Rytov variance equation (27), which classifies atmospheric fluctuations. There was no evidence to support that the length of the year's months has bearing on whether a strong or saturated relationship exists between the highest temperatures for each month. While the results are approaching strong at the lowest temperatures. As demonstrated in section 2.2.3, the gamma-gamma model is a good fit for the data since it accounts for all atmospheric fluctuations.

Figure 3.17 shows the calculation of the beta and alpha coefficients of the gamma-gamma model, where the values change according to the type of weather fluctuations. Where all the extracted values and the graph of a fluctuations system fit accordingly to the classifications in Figure (2.2).

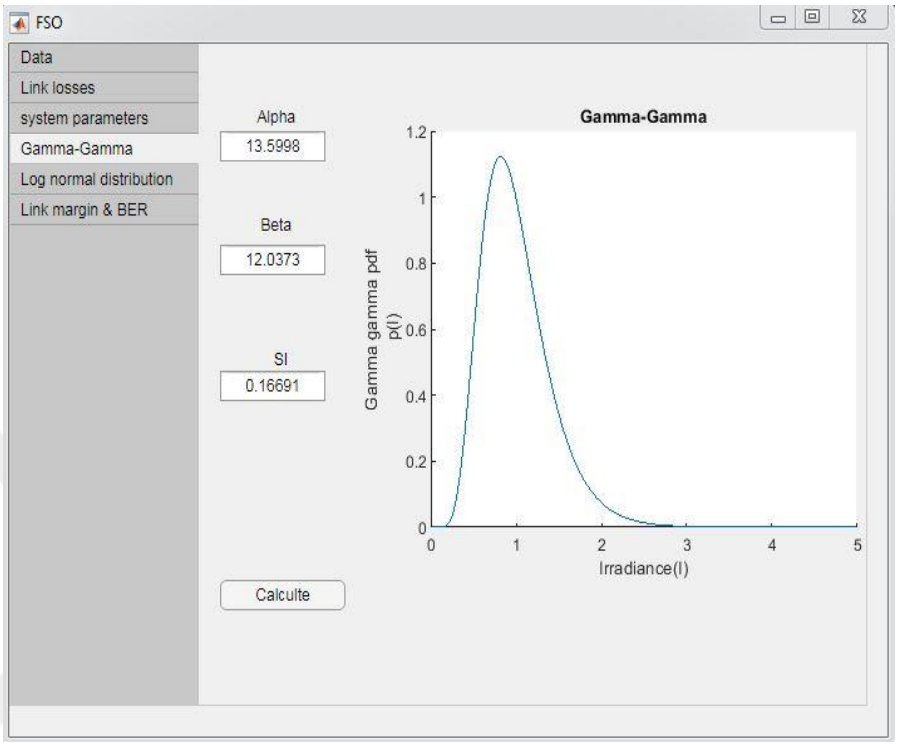

Figure 0.9. Calculation of the gamma-gamma model coefficients

Figure 3.18 shows several probability cases of intensity according to the type of fluctuations. The probability of the average variations of June's lowest temperature is shown in Figure 3.18a. August's greatest temperatures are shown in Figure 3.18. b., which presents the PDF in a strong condition. Figure 3.18.c resulted in the lowest temperatures occurring in April. At the hottest temperature, Figure 3.18.d displays the greatest rate computed.

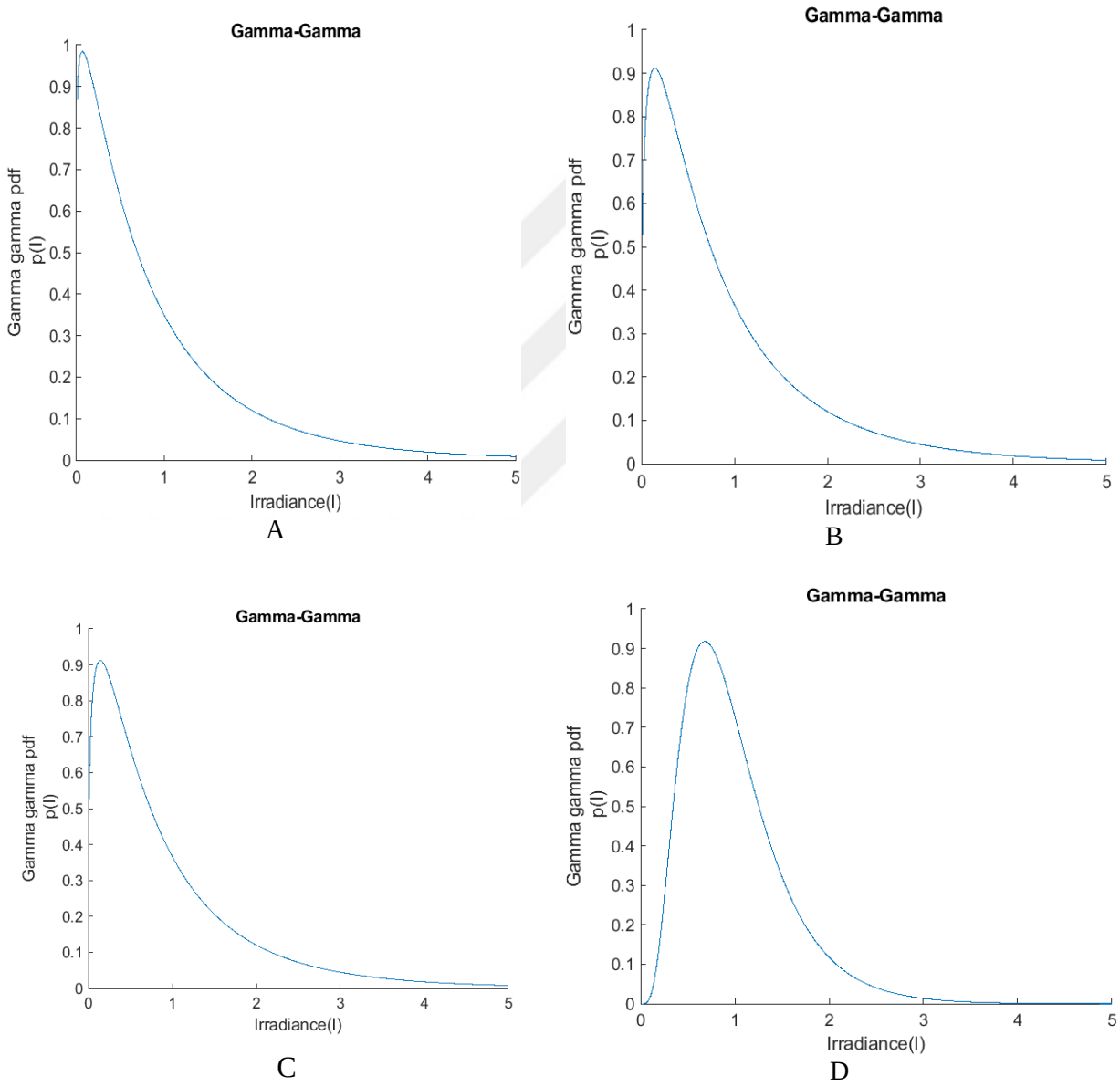

Figure 0.10. The probability of intensity according to the gamma-gamma model

3.4.1 Link Losses

In this section, the remaining attenuations subject to weather (fog, rain, snow) are calculated to see how they affect the proposed communication. The rate of snow and rain control the rate of attenuation, which can be calculated utilizing equations 32, 34, and 37. The annual average hourly rainfall and snowfall in the Kadiköy and Fatih areas, shown in figures 3.19 a, b. Calculating the average monthly intensity is as simple as multiplying the number of hours in the month by the number of months in the year(Hansen, 2019). The monthly average intensity in mm/h for both locations is shown in Table 3.2.

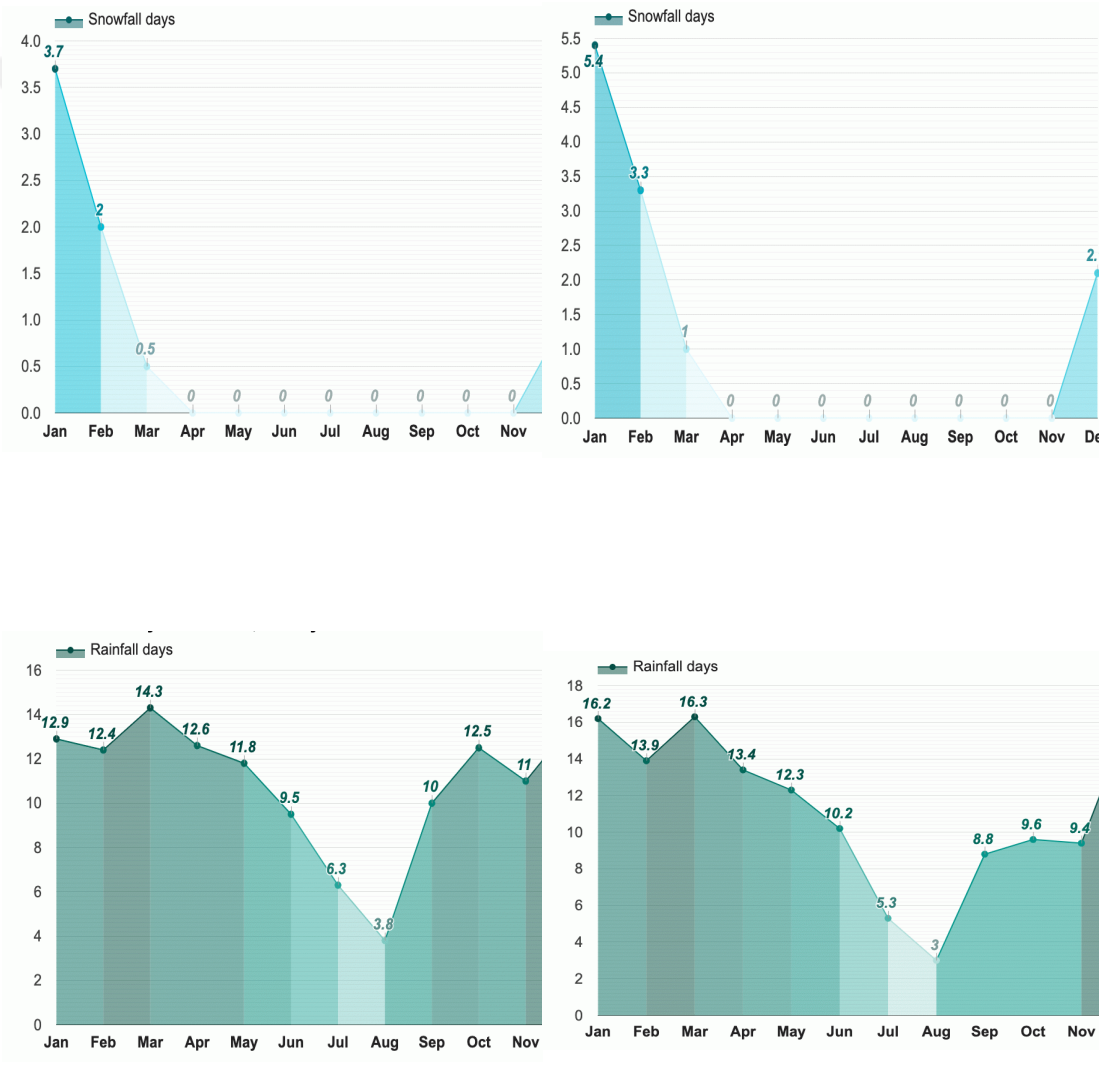

A B

Figure 0.119. A.Fatih falldays B. Kadikoy falldays("www.weather-atlas.com-istanbul", y.y.)

The amounts of rain and snowfall that occur monthly in the districts of Kadikoy and Fatih are outlined in Table 3.2.

Table 0.2. Average monthly intensity

Months	Kadikoy mm/h		Fatih mm/h	
	Rainfall	Snowfall	Rainfall	Snowfall
Jan	0.189119	0.620968	0.164983	0.303797
Feb	0.190031	0.653333	0.126712	0.3125
Mar	0.121447	0.625	0.112094	0.6
Apr	0.10443	0	0.098639	0
may	0.140893	0	0.139706	0
Jun	0.082645	0	0.144796	0
Jul	0.098361	0	0.088435	0
Aug	0.111111	0	0.1375	0
Sep	0.085	0	0.108333	0
Oct	0.162162	0	0.143345	0
Nov	0.136364	0	0.125	0
Dec	0.209845	0.755102	0.163522	0.777778

Figure 3.20 shows the link losses tab of the application, (visibility, rainfall, snowfall) were input into the program.

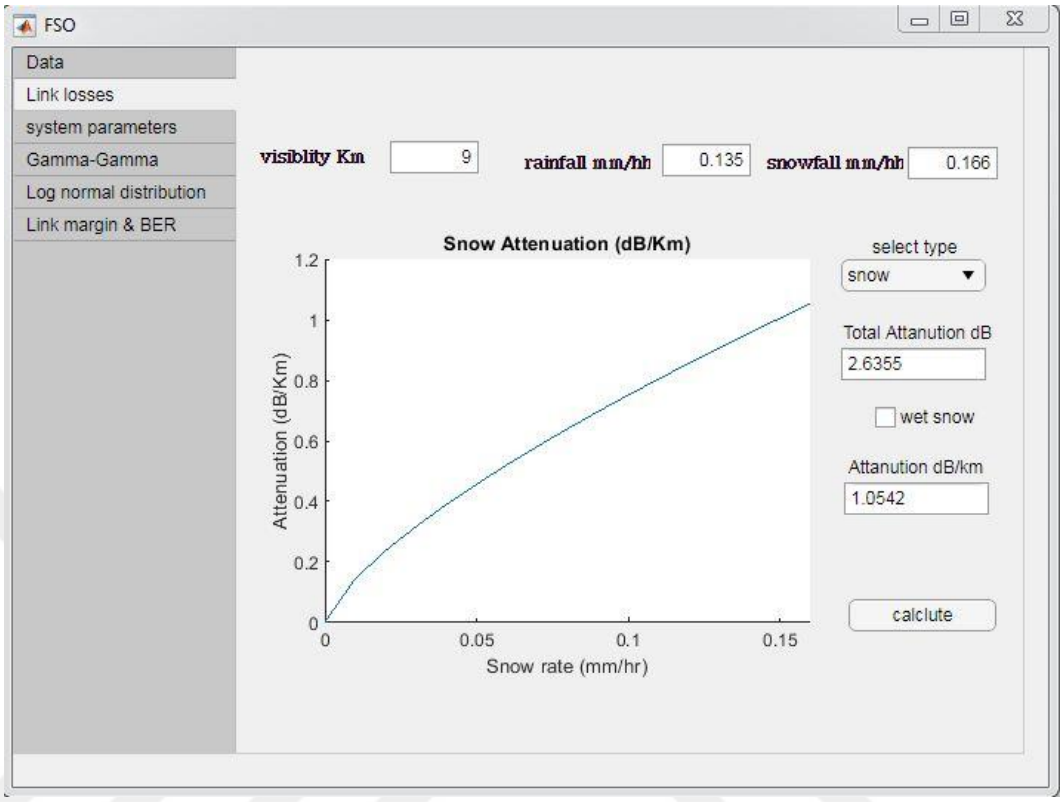

Figure 0.20 .Link losses calculation

The resultant attenuation values for each month and year are listed in table 3.3. The greatest attenuation values occurred in December in Kadiköy and the lowest values occurred in June and September in the Kadiköy area.

Table 0.3. Monthly link losses for Kadikoy and Fatih districts

Months	Kadikoy					Fatih				
	Snow dB	Snow dB/km	Rain dB	rain dB/km	Visibility dB	Snow dB	Snow dB/km	Rain dB	rain dB/k	Visibility dB
Jan	4.14	1.657	0.4	0.16	0.49	6.98	2.795	0.43	0.172	0.49
Feb	4.24	1.697	0.33	0.133	0.49	7.23	2.892	0.44	0.178	0.49
Mar	6.82	2.73	0.31	0.126	0.44	6.98	2.795	0.33	0.133	0.49
Apr	0	0	0.27	0.111	0.44	0	0	0.29	0.119	0.44
May	0	0	0.35	0.14	0.44	0	0	0.36	0.147	0.44
Jun	0	0	0.36	0.147	0.44	0	0	0.25	0.103	0.44
Jul	0	0	0.25	0.103	0.44	0	0	0.27	0.111	0.44
Aug	0	0	0.35	0.14	0.44	0	0	0.31	0.126	0.44
Sep	0	0	0.29	0.119	0.44	0	0	0.25	0.103	0.44
Oct	0	0	0.36	0.147	0.44	0	0	0.4	0.16	0.44
Nov	0	0	0.33	0.133	0.44	0	0	0.35	0.14	0.44
Dec	8.16	3.267	0.4	0.16	0.44	8.01	3.206	0.46	0.184	0.49
Mean	2.63	1.054	0.33	0.133	0.448333	3.31	1.325	0.35	0.14	0.456667

Snow attenuation rates in Fatih varied from 1.5 to 2.6 dB, whereas the maximum rain attenuation values were found between January and September. The highest snow attenuation rate was in March, with a value of 2.7 dB, and the months from April to October came at a rate of zero, due to the cessation of snowfall during that period.

3.4.2 Link Margin at the Linking Site

Link margin can be calculated from Equation 28 because it's a key component in determining how the system will behave in various weather conditions. In the preceding paragraph, the link loss was computed, which is dependent on the weather. The rest of the parameters are related to the system, such as the transmitting power, and the area of the receiving part. The molecular attenuation values (Att mol) can be simply calculated from Table 2.1 depending on the wavelength used in the transmission because the wavelength of 1550 nm has the least attenuation (0.01dB). The most important parameter in the link margin calculation is the geometric attenuation (Att Geo). According to Equation 29, the geometric attenuation is influenced by the distance, beam, and receiving area. Therefore, to improve any system properties, one of these factors can be changed to get the best results.

The resulting changes in Att(Geo) are obtained and shown in Fig 3.21 For a distance of 2.5 kilometers, the geometry attenuation is (35.92 dB), which has the greatest impact on the FSO's connection.

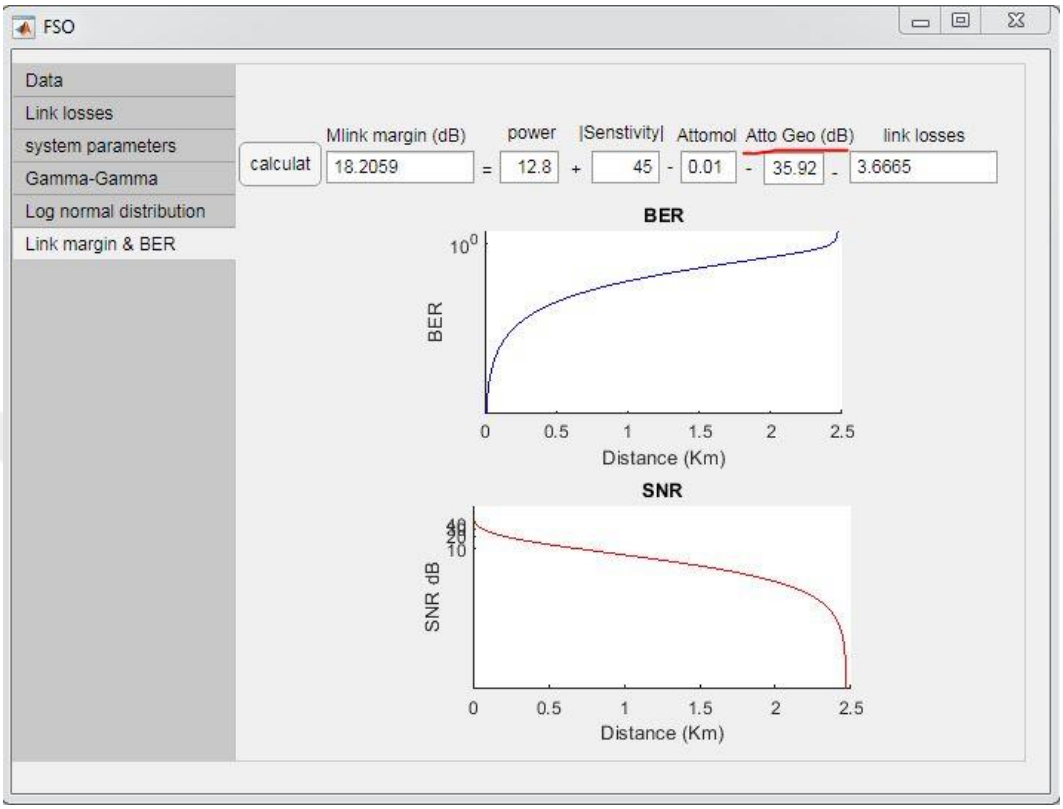

Figure 0.121. Calculation of geometric attenuation

Figure 3.22 shows the effect of changing the beam divergence and the capture area for the receiver, which can control geometric attenuation. As shown in figure (3.22. a) by reducing the divergence from two to one milliradian, the signal attenuation decreases by (6.1 dB). Moreover, when decreasing mrad to 1 the attenuation decreased to 29.89 dB as in Figure (3.22. b). Figure (3.22. c) shows that when beam divergence 2 mrad is held constant and the value of the capture area is changed from 0.08 to 0.1 m, the geometric attenuation becomes 33.97 dB. When the capture area was changed to 0.2 in Figure (3.22.d), the attenuation percentage was 27.95 dB.

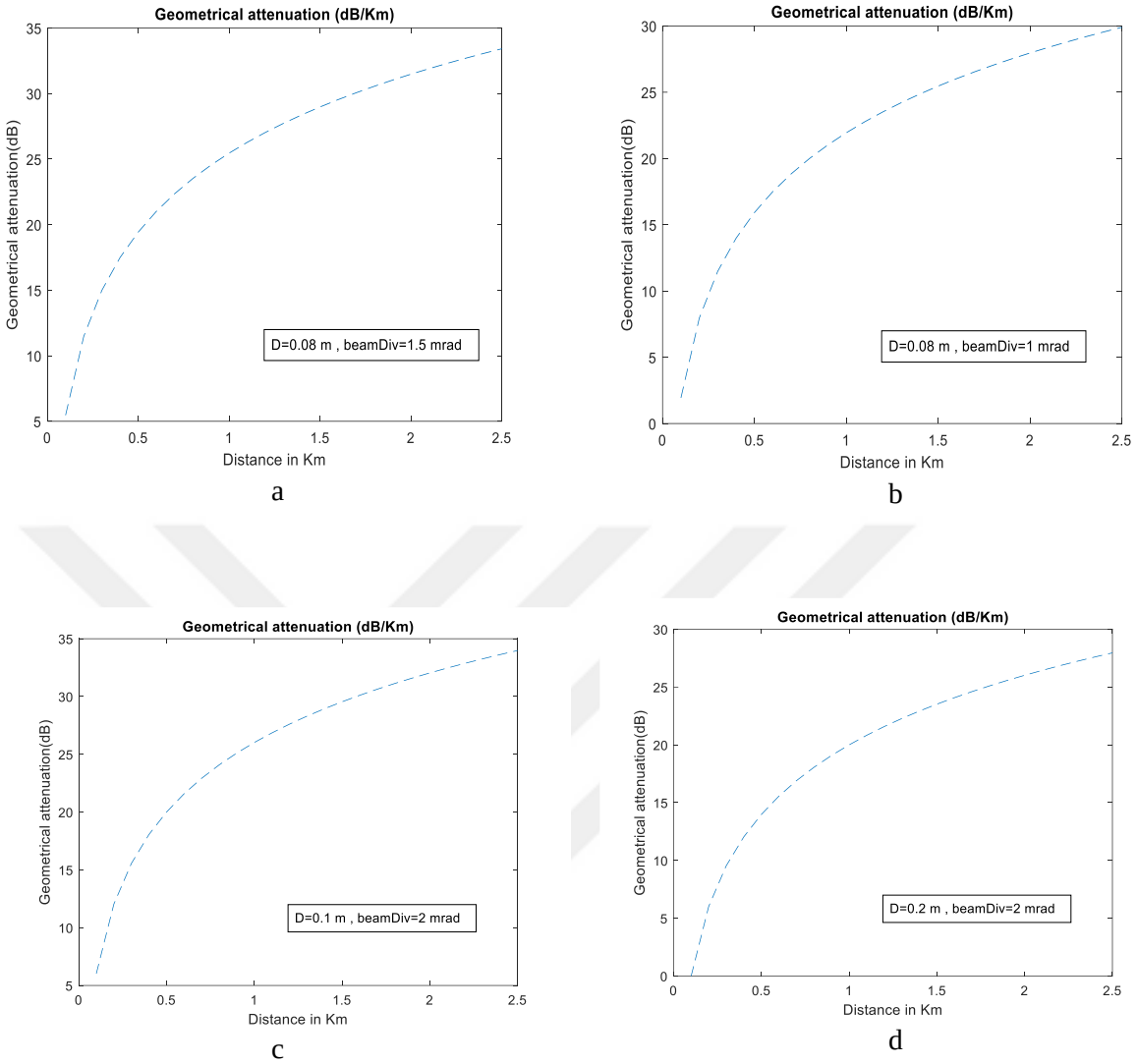

Figure 0.132. The Effect Of Beam and Capture Area On The Geometric Attenuation

In Figure (3.23), the best results were combined to reduce the attenuation to 21.93dB. When the divergence is 1 mrad, the capture area in the receiver increases to 0.2 m.

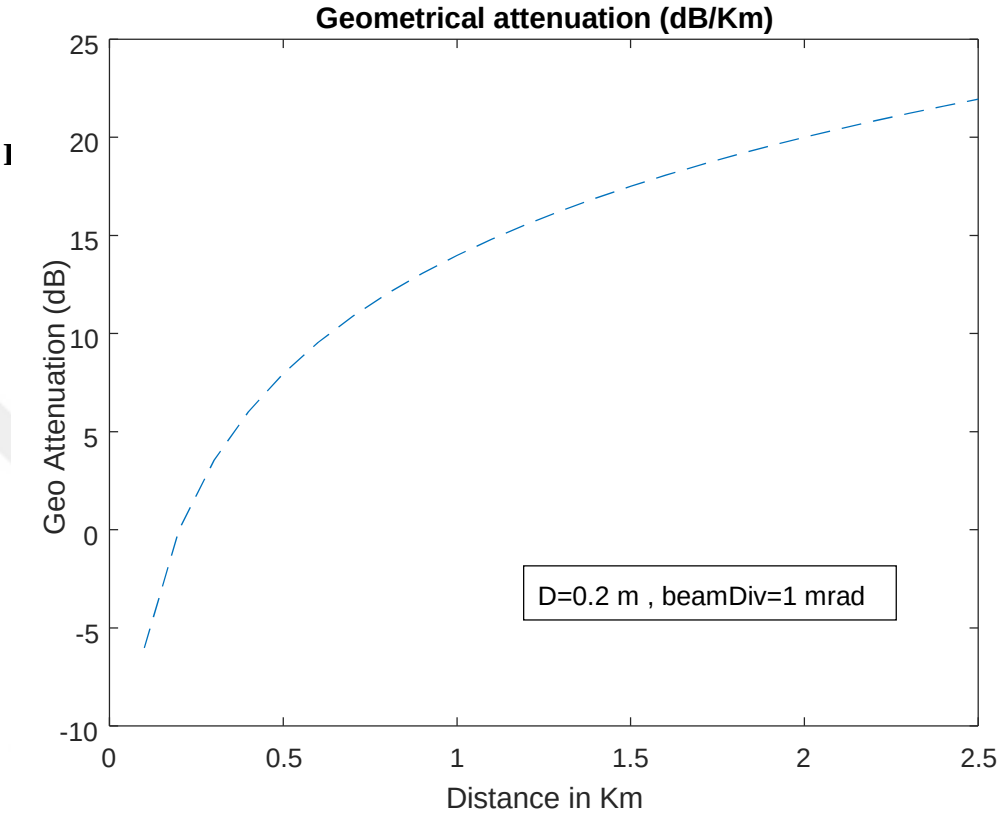

Figure 0.153. Geometrical attenuation after combining the best divergence and capturing area

The Link Margin for the year was estimated as shown in Figure 3.24, at geometric attenuation of (21.93 dB), 1 mrad divergence, and a capture area of 0.2 meters. The geometric attenuation was computed using the data in Table 3.3, which shows the total losses for the year. The quietest month is December, at (29 dB), followed by March, at (30.07 dB), February, at (30.9 dB), and January, at 31 decibels. From April to November, the average annual noise level was (35 dB).

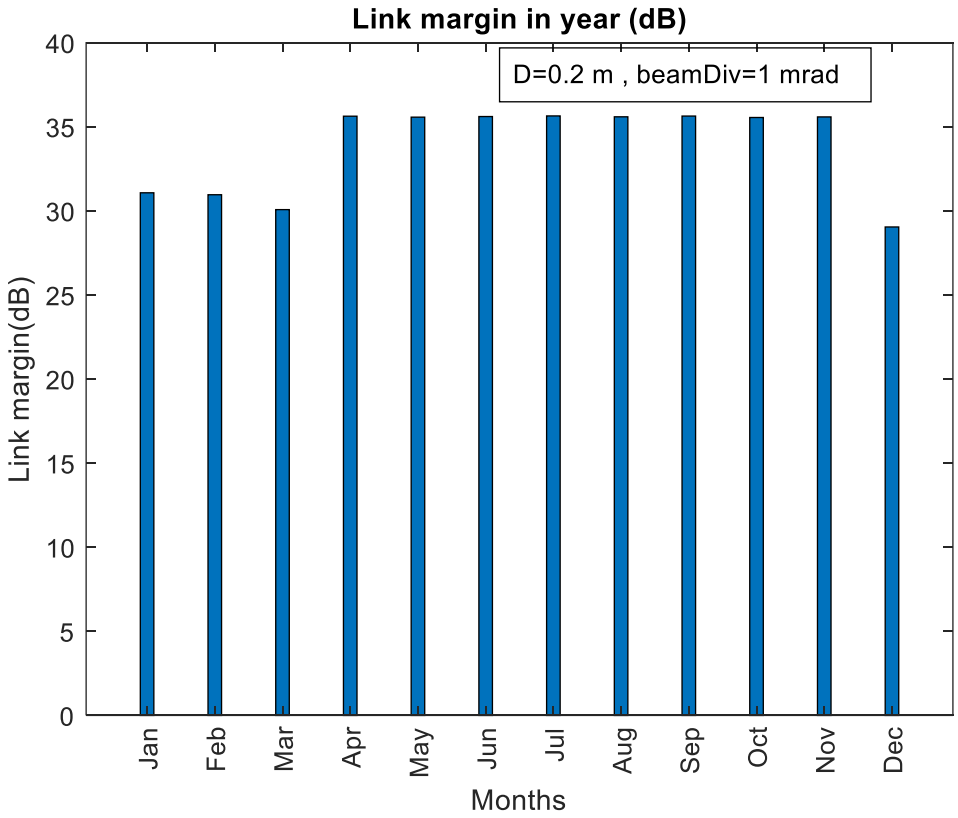

Figure 0.164. Link margin in year

CONCLUSION AND FUTURE WORKS

Conclusion

Wireless networks have increased their transmission capacity as well as their coverage area as a result of the continous demand for high-speed networks for a larger number of users accessing the service at the same time. To reduce spectral congestion in (interactive, lower frequency bands, ultramodern broadband, and multimedia services through wireless media), mobile and fixed cell networks have lately trended toward smaller cells and millimeter-wave frequency bands.

Additionally, FSO technology offers fast data speeds, low power consumption, compact size, as well as cheap prices for satellite cross-links. For a large network that operates as a high-speed trunking backbone for space networks, enabling mobile users and offering high data, services for small satellite terminals. Using decreasing weight, system complexity, and power for space systems helps minimize the cost of physical-link communication. With a laser device, FSO technology can be applied to roofs, buildings, and workplaces. All that is required is an optical transceiver with a laser transceiver to enable the full-duplex transmission capabilities of the FSO devices.

Lenses transmit light through the environment to other lenses that receive information in FSOs using high-power optical sources. All point-to-point, network, or point-to-multipoint FSO architectures are possible. It is also the data that may be sent between transmitters, receivers, or link heads using FSO systems over distances ranging from a few hundred meters to a few kilometers, depending on atmospheric conditions.

However, there are many limitations to the performance of FSO systems that limit their usefulness for some broadband network needs. The internal and external parameters of the FSO system must be taken into account. Rain, dust, snow, fog, and smoke are the most important external factors as they degrade the transmission path and cause network disruption. When creating an FSO system, these environmental changes must be taken into account. Internal factors include optical power, transmitting bandwidth, spacing angle, transmitter-side optical loss, BER, and receiver lens diameter.

In this study, some of the channel models used in the analysis of FSO links were reviewed. Negative exponential is used for significant turbulence and long-distance travel, log–normal is used for weak turbulence, Gamma-Gamma is used for all types of turbulence, and K-distribution for high turbulence. The most crucial system characteristics are the refractive index structure (C_n^2), which identifies the turbulence type. As well as from the relation between (C_n^2), and a structural parameter (CT) can calculate the variance value σ_R^2 to determine the scintillation index (SI), which classifies the kind of fluctuation. System variables such as geometric and molecular attenuation are indicated, like connection losses, rate of visibility, and how the coefficient (q) impacts the values of attenuation according to visibility range and its link to hazy attenuation, as well as calculating the amount of attenuation by wavelength. Furthermore, the rate of rain attenuation and its connection with precipitation quantities per hour (mm/h) had been categorized as the coefficients based on the quantity of precipitation. In addition, the characteristics of snow have a relationship to the rate of precipitation to calculate the snow attenuation.

In the third chapter, an FSO link for Istanbul is suggested. Because of its geographical location, which links the two continents (Asia - Europe), and the presence of climatic diversity, it is nominated as a suitable place to study the climatic factors on the link. The real data was taken for the areas (Fatih - Kadikoy) on both sides of the Bosphorus Strait, a distance of 2.5 km. The data was the annual average for both areas of temperature (maximum-minimum), atmospheric pressure, wind speed, visibility, rain, and snowfall rate. Where the provided data was processed by a Matlab-programmed application that calculated the influence of the weather and described the kind of turbulence according to the system characteristics and determined the right model for the connection.

The findings were calculated using air pressure data and temperature differences to get the coefficient (C_n^2). Atmospheric turbulence becomes strong, often at lower temperatures, and on the contrary, turbulence is moderate to weak at higher temperatures throughout the year. The indicator of the coefficient (SI) values is based on the variance of sigma values. The fluctuations are subject to the same condition as the above. Where the fluctuations are strong to saturated at the lowest temperatures, and moderate to weak at the highest temperatures. As a result, a more reliable

connection is adopted throughout the day and at maximum temperatures. Because the link is situated in the turbulence zone and is distinct from the previous results, the likelihood of intensity was calculated using the (gamma-gamma) model, which applies to all forms of turbulence. Alpha-beta coefficients were calculated for four cases (weak, moderate, strong, and linkage rate) for the annual suggested linkage rate.

Link losses are calculated in a unit (mm / h) for the rates of rain and snowfall using the same application to calculate the annual, average attenuation rates per km and the total distance of the connection. It appeared that the months of April-November are the least attenuated because of the low rates of rain and the cessation of snow. However, the rate of attenuation of visibility did not affect the connection for the length of the year.

The link margin was calculated after entering all the variables such as transmit power, sensitivity, and wavelength. It was found that the geometric attenuation rate has the most influence on the connection. The divergence was lowered from (2 mrad) to (1 mrad) and the area of capture was raised from (0.08 to 0.2 m) to lessen this impact, with the consequence that the geometric attenuation was reduced by a (10 dB). The average yearly linkage margin is determined by the geometric and weather attenuations. The weather was often mild throughout the year in recommended sites, with April to November being the most favorable meteorological conditions for the connection process.

From the results that we obtained in the study, we can consider the recommended site for linking. Successful use of FSO techniques and the obstacles encountered by the system, whether technical or natural, can be dealt with by changing the characteristics of the transmitter or receiver. Because the weather in the connecting region is often good.

Unpredictable weather factors can also have a significant impact on the communication process. The research also does not take into account to address the issues of misalignment and direction, which are regarded to be a factor determining

the connection's effectiveness. This research was developed theoretically to assess the FSO link process as a proposed alternative to other procedures due to the high prices of equipment and the lengthy time necessary to examine all weather elements.

Future Work

From the presented study, it was found that all the results were theoretically taken, and a simulation was made to analyze the system using a computer software program. Therefore, a practical study on site will be an important part of evaluating the communication process and testing. That will further validate the results that were obtained from the Matlab application.

Alternatively, the proposed FSO link could be applied to a different geographical location that would present new variables and challenges for the software introduced previously.

In addition, the suggested link could be made underwater using underwater wireless optical communication (UWOC) which is known to have high baud, short-range wireless links, low latency, and energy efficiency. Furthermore, Istanbul city has access to multiple seas, the addition of an FSO-based link connecting the city to surrounding islands. Beam absorption, dispersion, and underwater turbulence are the primary problems limiting the (UWOC) systems. These factors should be studied, and analyzed.

Finally, having an accurate pattern of losses can help mitigate them in the design process, FSO link attenuations could be predicted using modern technologies such as Artificial Intelligence, therefore, it is recommended to research FSO attenuations pattern recognition prediction using AI.

REFERENCES

Al Naboulsi, M. C. (2004). Fog attenuation prediction for optical and infrared waves. *Optical Engineering,* , 43(2), 319-329.

Al Naboulsi, M. C. (2004). Wavelength selection for the free space optical telecommunication technology. *In Reliability of Optical Fiber Components, Devices, Systems, and Networks* , (Vol. 5465, pp. 168-179).

Al Naboulsi, M. C. (2004). Wavelength selection for the free space optical telecommunication technology. *In Reliability of Optical Fiber Components, Devices, Systems, and Networks II* , (Vol. 5465, pp. 168-179).

Alheadary, W. G. (2018). Free-space optical channel characterization and experimental validation in a coastal environment. *Optics Express,*, 26(6), 6614-6628.

Arockia Bazil Raj, A. &. (2016). Statistical analysis of accurate prediction of local atmospheric optical attenuation with a new model according to weather together with beam wandering compensation system: a season-wise experimental investigation. *Journal of Modern Optics,*, 63(13), 1286-1296.

Awan, M. S. (2009). Weather effects impact on the optical pulse propagation in free space. *In VTC Spring 2009-IEEE 69th Vehicular Technology Conference* (pp. (pp. 1-5)). IEEE.

Barnett, T. J. (2018). Cisco visual networking index (vni) complete forecast update. *Americas/EMEAR Cisco Knowledge Network (CKN) Presentation*.

Barua, B. &. (2011). Evaluate the performance of FSO communication link with different modulation technique under turbulent condition. *In 14th International Conference on Computer and Information Technology (ICCIT 2011)* (pp. (pp. 191-195)). IEEE.

Bates, D. R. (1984). Rayleigh scattering by air. *Planetary and Space Science,*, 32(6), 785-790.

Begley, D. L. (1992). *Free-Space Laser Communication Technologies IV*.

Bell, A. G. (1880). Upon the production and reproduction of sound by light. *Journal of the Society of Telegraph Engineers,*, 9(34), 404-426.

Bhatnagar, M. R. (2016). Performance analysis of gamma–gamma fading FSO MIMO links with pointing errors. *Journal of Lightwave technology*, 34(9), 2158-2169.

Bloom, S. K. (2003). Understanding the performance of free-space optics. *Journal of optical Networking,*, 2(6), 178-200.

Borah, D. K. (2012). A review of communication-oriented optical wireless systems. *EURASIP Journal on Wireless Communications and Networking*, 1-28.

Bouchet, O. B. (2008). Indoor Free Space Optic: A new prototype, realization and evaluation. *In Free-Space Laser Communications VIII* (pp. (Vol. 7091, pp. 118-126).). SPIE.

Bouchet, O. E. (2008). Hybrid wireless optics (HWO): Building the next-generation home network. *In 2008 6th International Symposium on Communication Systems, Networks and Digital Signal Processing* (pp. (pp. 283-287).). IEEE.

Bouchet, O. M. (2005). FSO and quality of service software prediction. *International Society for Optics and Photonics.*, V (Vol. 5892, p. 589204).

Bouchet, O. S. (2010). Free-space optics: propagation and communication. *John Wiley & Sons.*, (Vol. 91).

Cao, Q. B.-P. (2006). CTH07-5: Free space optical mimo system using an optical pre-amplifier. *In IEEE Globecom*, (pp. 1-5).

Chabane, M. A. (2004). A new quality of service FSO software. *Reliability of Optical Fiber Components, Devices, Systems, and Networks II* , (Vol. 5465, pp. 180-187).International Society for Optics and Photonics.

Chan, V. W. (2003). Optical satellite networks. . *journal of Lightwave Technology,*, 21(11), 2811.

Chia, S. G. (2009). The next challenge for cellular networks. *Backhaul. IEEE Microwave Magazine*, 10(5), 54-66.

Choi, S. Y. (2018). A comparison of ICS datasets for security research based on attack paths. *In International Conference on Critical Information Infrastructures Security* (pp. (pp. 154-166)). Springer,.

Fadhil, H. A.-K. (2013). Optimization of free space optics parameters: An optimum solution for bad weather conditions. *Optik, ,* 124(19), 3969-3973.

Farid, A. A. (2007). Outage capacity optimization for free-space optical links with pointing errors. *Journal of Lightwave technology*, 25(7), 1702-1710.

Farid, A. A. (2007). Outage capacity optimization for free-space optical links with pointing errors. *Journal of Lightwave technology,*, 25(7), 1702-1710.

Farooq, E. S. ((pp. 255-264).). Survey on FSO communication system—Limitations and enhancement techniques. *In Optical and wireless technologies* , 2018.

Farooq, E. S. (2018). Survey on FSO communication system—Limitations and enhancement techniques. *In Optical and wireless technologies*, (pp. 255-264).

Gfeller, F. R. (1979). Wireless in-house data communication via diffuse infrared radiation. *Proceedings of the IEEE,*, 67(11), 1474-1486.

Ghassemlooy, Z. P. (2019). *optical wireless communications: system and channel modelling with Matlab®.* CRC press.

Ghassemlooy, Z. P. (2019). *Optical wireless communications: system and channel modelling with Matlab®.* CRC press.

Gohil, A. (2019). *Free Space Optical Communication.*

Goodwin, F. E. (1970). A review of operational laser communication systems. *Proceedings of the IEEE,*, 58(10), 1746-1752.

Gradshteyn, I. S. (2014). Table of integrals, series, and products. . *Academic press.*

Guo, H. L. (2010). Influence of beam wander on uplink of ground-to-satellite laser communication and optimization for transmitter beam radius. *Optics letters,*, 35(12), 1977-1979.

Haas, H. (2011). Wireless data from every light bulb.

Hemmati, H. (2006). *Deep space optical communications.* John Wiley & Sons.

Horimai, H. T. (2005). Collinear holography. *Applied optics,*, 44(13), 2575-2579.

Hou, K. S. (2002). A differential coding method for the symmetrically differential polarization shift-keying system. *IEEE transactions on communications,*, 50(12), 2042-2051.

Hranilovic, S. &. (2004). Short-range wireless optical communication using pixilated transmitters and imaging receivers. *In 2004 IEEE International Conference on Communications (IEEE Cat. No. 04CH37577)* (pp. Vol. 2, pp. 891-895).). IEEE.

Huang, H. X. (2014). 100 Tbit/s free-space data link enabled by three-dimensional multiplexing of orbital angular momentum, polarization, and wavelength. *Optics letters, ,* 39(2), 197-200.

Huang, T. Y. (2019). A survey on green 6G network: Architecture and technologies. *IEEE access*, 7, 175758-175768.

Jakeman, E. &. (1976). A model for non-Rayleigh sea echo. *IEEE Transactions on antennas and propagation, ,* 24(6), 806-814.

Jakeman, E. &. (1978). Significance of K distributions in scattering experiments. *Physical Review Letters,*, 40(9), 546.

Jeong, M. C. (2002). 8× 10 Gb/s terrestrial optical free space transmission over 3.4 km using an optical repeater. *In Optical Fiber Communication Conference (p. ThD4)*. Optical Society of America.

Karp, S. G. (2013). Optical channels: fibers, clouds, water, and the atmosphere. *Springer Science & Business Media*.

Kaushal, H. &. (2015). Free space optical communication: challenges and mitigation techniques. *arXiv preprint arXiv:1506.04836*.

Kaushal, H. K. (2011). Experimental study on beam wander under varying atmospheric turbulence conditions. *IEEE Photonics Technology Letters,*, 23(22), 1691-1693.

Kerr, J. R. (1972). Experiments on turbulence characteristics and multiwavelength scintillation phenomena. *JOSA,*, 62(9), 1040-1049.

Kiasaleh, K. (2005). Performance of APD-based, PPM free-space optical communication systems in atmospheric turbulence. *IEEE transactions on communications,* , 53(9), 1455-1461.

Kiasaleh, K. (2006). Performance of coherent DPSK free-space optical communication systems in K-distributed turbulence. *IEEE transactions on communications,*, 54(4), 604-607.

Kruse, P. W. (1962). *Elements of infrared technology: Generation, transmission and detection*. New York: Wiley.

Kumar, P. &. (2015). Enhanced performance of FSO link using OFDM and comparison with traditional TDM-FSO link. *In 2015 IEEE International Broadband and Photonics Conference (IBP)* (pp. (pp. 65-70).). IEEE.

Lee, S. K. (2012). Evaluation of visible light communication channel delay profiles for automotive applications. . *EURASIP journal on Wireless Communications and Networking*, 1-8.

Long, R. K. (1963). Atmospheric attenuation of ruby lasers. *Proceedings of the IEEE,*, 51(5), 859-860.

Majumdar, A. K. (2010). Free-space laser communications: principles and advances. *Springer Science & Business Media.*, (Vol. 2).

Manohar, S. &. (2016). Photoacoustics: a historical review. *Advances in optics and photonics,*, 8(4), 586-617.

Muhammad, S. S. (2005). Channel modeling for terrestrial free space optical links. *In Proceedings of 2005 7th International Conference Transparent Optical Networks*, (pp. (Vol. 1, pp. 407-410).). IEEE.

Niaz, A. Q. (2019). Performance analysis of chaotic FSO communication system under different weather conditions. . *Transactions on Emerging Telecommunications Technologies,*, 30(2), e3486.

Pan, G. E. (2011). Capacity analysis of log-normal channels under various adaptive transmission schemes. *IEEE communications letters,*, 16(3), 346-348.

Pan, G. E. (2011). Capacity analysis of log-normal channels under various adaptive transmission schemes. *IEEE communications letters, ,* 16(3), 346-348.

Pang, G. H. (1999). Visible light communication for audio systems. *IEEE Transactions on Consumer Electronics,*, 1112-1118.

Parikh, J. &. (2011). Study on statistical models of atmospheric channel for FSO communication link. *In 2011 Nirma University International Conference on Engineering IEEE.* (pp. (pp. 1-7).). IEEE.

Peppas, K. N. (2012). Performance analysis of SISO and MIMO FSO communication systems over turbulent channels. *Optical communication, ,* 415-438.

Roberts, R. D. (2013). Space-time forward error correction for dimmable undersampled frequency shift ON-OFF keying camera communications (CamCom). *In 2013 Fifth International Conference on Ubiquitous and Future Networks (ICUFN)* (pp. (pp. 459-464).). IEEE.

Rodewald, D. (2008). MRV introduces industry's first 10G ethernet wireless point-to-point system. *MRV Communications, Inc.*

Sannibale, V. O. (2009). A sub-hertz vibration isolation platform for a deep space optical communication transceiver. *International Society for Optics and Photonics.*

Sari, F. &. (2011). Optical wireless communications: Link availability prediction for the city of Istanbul. *In Proceedings of the 11th International Conference on Telecommunications* (pp. (pp. 207-210).). IEEE.

Scholz, R. F. (2016). Undergraduate experiments on statistical optics. *European Journal of Physics,*, 37(5), 055302.

Schütz, I. F. (1990). Miniature self-frequency-doubling cw Nd: YAB laser pumped by a diode-laser. *Optics communications*, 77(2-3), 221-225.

Sharma, T. C. (2021). Review of optical and wireless backhaul networks and emerging trends of next generation 5G and 6G technologies. *Transactions on Emerging Telecommunications Technologies*, 32(3), e4155.

systems, M.-C.-b. c. (2013). Monte-Carlo-based channel characterization for underwater optical communication systems. *ournal of Optical Communications and Networking*,, 5(1), 1-12.

Tang, X. R. (2010). Performance of BPSK subcarrier intensity modulation free-space optical communications using a log-normal atmospheric turbulence model. *In 2010 Symposium on Photonics and Optoelectronics*, (pp. 1-4).

Tatarski, V. I. (1961). *Wave Propagation in a Turbulent Medium 1Dover*. . ew York, 19612, 147.

Taubenblatt, M. A. (2011). Optical interconnects for high-performance computing. *Journal of Lightwave Technology*,, 30(4), 448-457.

Tipmongkolsilp, O. Z. (2010). The evolution of cellular backhaul technologies: Current issues and future trends. . *IEEE Communications Surveys & Tutorials*, 13(1), 97-113.

Tsiftsis, T. A. (2009). Optical wireless links with spatial diversity over strong atmospheric turbulence channels. *IEEE transactions on wireless communications*,, 8(2), 951-957.

turbulence, B. s.-s. (2009). BPSK subcarrier intensity modulated free-space optical communications in atmospheric turbulence. *Journal of Lightwave technology*, , 27(8), 967-973.

Tyler, G. A. (1994). Bandwidth considerations for tracking through turbulence. *JOSA A*,, 11(1), 358-367.

Uysal, M. &. (2014). Optical wireless communications—An emerging technology. *In 2014 16th international conference on transparent optical networks (ICTON)* (pp. (pp. 1-7)). IEEE.

Uysal, M. &. (2014). Optical wireless communications—An emerging technology. *In 2014 16th international conference on transparent optical networks (ICTON)* (pp. (pp. 1-7).). IEEE.

Wang, Z. Z. (2009). Performance comparison of different modulation formats over free-space optical (FSO) turbulence links with space diversity reception technique. *IEEE Photonics Journal,*, 1(6), 277-285.

Weichel, H. (1990). *Laser beam propagation in the atmosphere.* SPIE press.

Wilfert, O. K. (2010). Propagation study of 850nm/58 GHz hybrid municipal system. *In Free-Space Laser Communications X*, (Vol. 7814, pp. 301-308). SPIE.

Willebrand, H. &. (2002). *Free space optics: enabling optical connectivity in today's networks.* SAMS publishing.

Willebrand, H. &. (2002). *Free space optics: enabling optical connectivity in today's networks.* SAMS publishing.

Wu, Z. C. (2011). Modeling and designing of a new indoor free space visible light communication system. *In 2011 16th European Conference on Networks and Optical Communications* (pp. (pp. 72-75)). IEEE.

Yan, J. Z. (2006). Improved performance of M-ary PPM free-space optical communication systems in atmospheric turbulence due to forward error correction. *In 2006 International Conference on Communication Technology* (pp. (pp. 1-4).). IEEE.

Zhang, W. &. (1999). *Power-law parameters of rain specific attenuation.*

Zhongming, Z. L. (2018). *Simulating the refractive index structure constant (Cn2) in the surface layerat Antarctica with a Mesoscale mode.*

Zong, B. F. (2019). 6G technologies: Key drivers, core requirements, system architectures, and enabling technologies. *IEEE Vehicular Technology Magazine,*, 14(3), 18-27.